When to Lock, Not Whom: Managing Epidemics Using Time-Based Restrictions*

Yinon Bar-On, Weizmann Institute of Science, Israel
Tanya Baron, Ben Gurion University, Israel
Ofer Cornfeld, BFI, Israel
Ron Milo, Weizmann Institute of Science, Israel
Eran Yashiv, Tel Aviv University, Israel; CfM (LSE), UK; and CEPR†

March 16, 2021

Abstract

We present normative and positive analyses of policy tools to manage epidemics, both current and any future ones.

Against the background of serious misspecification of COVID19 dynamics in Economics research, at odds with the evidence, we present a constructive alternative with a sound model. This may guide researchers and place the analysis in Economics on solid footing.

We introduce novel NPI tools for the management of epidemics. Rather than using prevalent policies based on *population* restrictions, these place *time* at the center of the analysis: time restrictions, relation to timescales of virus transmission, and optimal timing of interventions.

Key findings are that the new tools significantly improve social welfare, substantially lessening the trade-offs involved; optimally-derived timings of interventions suppress the disease while maintaining reasonable economic activity; and outcomes are superior to the actual experience of New York State and Florida in the course of 2020.

Key words: public health policy, NPI, roles of time, normative analysis, positive analysis, epidemic/pandemic management, virus timescales, SEIR model, policy frontier.

JEL codes: E23, E61,E65, I12, I18

We thank Philipp Kircher, Marc Lipsitch, and Ben Moll for useful exchanges, seminar participants at UCL, LSE, and Tel Aviv for comments, and Roy Cnaan for research assistance. Any errors are our own.

†*Corresponding author.* yashiv@tauex.tau.ac.il; phone +972-3-640-9233; fax +972-3-640-9908; The Eitan Berglas School of Economics, Tel Aviv University, Tel Aviv 6997801, Israel.

When to Lock, Not Whom:
Managing Epidemics Using Time-Based Restrictions

1 Introduction

Since March 2020 there has been a rapidly expanding research effort dedicated to COVID19 analysis across disciplines, inter alia, in Economics. This comes against the background of the pandemic having created a global health and economic crisis of a magnitude not experienced since the Great Influenza Pandemic of 1918-1919. After a year, the death toll in the U.S. is around $530,000$, and the declines in U.S. GDP and consumer expenditures for 2020 have been -3.5% and -3.9%, respectively. A typical analysis posits a planner problem that seeks to derive optimal policy – Non-Pharmaceutical Interventions (NPIs), and in particular, lockdowns – subject to a model of COVID19 dynamics. The planner trades off the costs of public health outcomes, such as breach of ICU capacity and death, with the economic costs of suppression policy, including declines in production. In the real world, the policy response across countries and U.S. states and over time has been volatile, heterogeneous, and, occasionally, erratic.

This paper offers two innovations.

One is a modelling contribution. It comes against the background of prevalent misspecification of disease dynamics in Economics research, at odds with the epidemiological evidence, explored in detail in a companion paper (Bar-On, Baron, Cornfeld, Milo, and Yashiv (2021)). We have shown that erroneous modelling has substantial consequences for policy. Two key properties of disease dynamics, its scale and speed, are at the center of misspecification. Here we present a constructive alternative with a sound model that may guide researchers and place the analysis in Economics on solid footing. We evidently eschew the cited modelling errors.

The second is that the paper introduces novel policy tools for pandemic or epidemic management, based on time restrictions. The proposed tools consist of alternating periods of work and lockdown, at pre-defined frequencies, for the entire population. The paper stresses the crucial multiple roles played by time in this context. We present both normative and positive analyses. The former applies to the management of the ongoing COVID19 pandemic, as well as to any future pandemic or epidemic. The latter evaluates policy against real world benchmarks in the U.S.

The novel tools are particularly relevant in light of the difficulties experienced by policymakers in finding a policy strategy that lessens the trade-offs involved. In theory, targeted population lockdowns could constitute "fine tuning " of lockdown measures, which would serve to lessen any economic cost. In practice, however, it turned out to be challenging to identify sub populations to be allowed unrestricted economic activity, while imposing restrictions on other population groups. Political and moral issues, as well as practical implementation issues, have come into play. This was made even more difficult by the

uncertainty with respect to the exact state and dynamics of the epidemic. The novel, time-based public health management policy avoids these difficulties, taking time, rather than population, as the medium of restrictions.

We highlight the following dimensions related to time:

(i) From the normative perspective, the paper analyzes novel policy that relies on *time restrictions*. Such policy is an alternative to policy based on restrictions of sectors, age groups, regions, or other targeted population groups. It is a cyclical strategy, using an alternating work and lockdown schedule for the whole population, to manage the epidemic ahead of full vaccine introduction.

(ii) The rationale for the proposed policy is directly based on the *timescales of virus transmission*. The essential idea is that for every 14 day period, there will be k days of work and $14 - k$ days of lockdown. This number, k, uses the timescales of the virus against itself, inter alia taking into account a latent period after exposure, whereby the infected person does not infect others. This policy follows epidemiologically-grounded work by Karin et al (2020). For future epidemics, a similar empirical logic would apply. We elaborate on this issue below.

(iii) Using an optimizing social planner model, the control variables for this policy are *the timing of the various measures* – initial lockdown, the cyclical policy phase, and release. Hatchett, Mecher, and Lipsitch (2007) highlight the idea that imposing NPIs early in an epidemic can significantly reduce mortality. In the current paper, the exploration of timing issues, both start time and duration, are at the heart of the analysis.

(iv) This policy is compared to a prevalent policy path which sets lockdown and release as *functions of disease prevalence, which is time-varying*. Specifically, the latter uses trigger thresholds, such as the number of persons hospitalized in ICU in a given period of time, and gives rise to the pattern of recurrent lockdown and release observed in the U.S. and other countries since the start of COVID19.

(v) The proposed policy is also compared to the actual experience of New York State (NYS) and Florida. The outcomes observed for these states turn out to depend crucially on *the timing of the policies undertaken.*

The model explicitly takes into account two important realistic elements: one is a dynamic path for the reproduction parameter, reflecting both rational individual behavior and the effects of suppression policy. We take into account that individuals adjust to the new environment and behave differently, both with and without government interventions. These changes happen in part as a direct result of government NPIs and in part as a voluntary response. We model this time variation by relying on data estimates.

The second is vaccine arrival. The planner uses a PDF to form ex-ante expectations of this arrival time. Specifically, the arrival time of the vaccine is modeled as a result of simultaneous competition among many firms, which is well approximated by a Gumbel distribution. In our simulations vaccine arrival is realized after 540 days. We note that, at the time of writing (March 2021), there has been considerable progress in vaccine development, authorization, and vaccination.

We simulate the optimal time-restrictions (cyclical) policies and examine their health and economic implications. The methodology is to find the values of three time points that minimize the planner cost function. We solve the continuous time system of ODE describing the stocks of population in different epidemiological and clinical states. The solution is obtained using a hierarchical search of the three-dimensional control variables space. We derive a set of interpolated functions describing the dynamics of all stocks, enabling us to evaluate the planner's objective.

The cyclical policy is compared to four non-cyclical benchmarks: two polar cases, of no policy intervention (i.e., no lockdown) or full lockdown till vaccine arrival; a single lockdown policy, whereby the starting date and the duration are chosen optimally; and a theoretical path trying to mimic real-world policy, whereby the planner chooses thresholds for multiple lockdowns in terms of the critically ill. We also evaluate the novel tools in relation to the 2020 experience of NYS and Florida. The latter comparison also allows us to check the validity of our model in the data, as we compare the NYS and Florida outcomes predicted by the model to the data.

We trace out a policy frontier consisting of outcomes of optimal planner policies under the cyclical instruments, using a two-dimensional graph of the death toll per 1 million people and the value of lost output, in annual GDP terms. Movement along the frontier occurs as the policy instrument in use changes, or as the weight assigned to fatalities in the planner objective function changes.

Our analysis yields the following key findings.

First, in terms of the policy frontier, for the most part a trade-off between health and economic outcomes is clear, with deaths rising and output loss falling with an almost constant proportion. Movement along the frontier is generated by variations in the stringency of interventions, either because the policy instruments used vary, or because a different relative weight is assigned to losses due to death. In short segments at the extremities, the frontier is almost vertical (where the death toll is low) and almost horizontal (where the death toll is high), implying no trade-off.

Second, the novel instruments, based on time restrictions, provide for significant improvement, substantially lessening the trade-offs involved relative to the four non-cyclical benchmarks. The latter are situated in points on the graph beyond the frontier.

Third, we quantify social welfare in terms of planner costs. These are given in Present Discounted Value (PDV) terms over two years, in units of GDP per annum. While the different cyclical strategies place these losses at 27% to 32% of annual GDP in PDV terms over two years, the no intervention policy results in 113%, full lockdown in 50%, optimal lockdown in 42%, and the thresholds strategy in 34% of annual GDP The underlying rationale for the improvement is that cyclical strategies allow the planner to achieve similar death tolls with fewer lockdowns, or to reduce the death toll dramatically without a significant damage to output. These results are due to the optimally-derived timings of intervention (for example, "front loading" interventions is beneficial in specific

cases, which are spelled out) and the ability of the cyclical strategies to suppress the disease while maintaining a reasonable level of economic activity.

Fourth, using daily data from March to November 2020, optimal cyclical policies fare much better than actual experience in the states of New York and Florida. While deriving this result, we confirm that the model is able to reproduce the data outcomes observed in each state, using state-specific parameters in the simulations.

Importantly, the benefits of the time-based policy tools that we find are likely to be a lower bound of their true advantage over strategies that have been implemented. This is so because, for tractability, we are not giving the planner full flexibility when applying the cyclical tools. Similarly, we do not quantify their additional benefits, such as predictability of production, gains in other health matters, transparency, ease of communication, and fairness.

We note that the idea of a cyclical strategy, which is at the focal point of the normative analysis of this paper, has been brought to the attention of policymakers (see Yashiv (2020), Alon and Yashiv (2020), and Alon, Milo and Yashiv (2020)) and has been considered or implemented by a host of firms and educational institutions in the U.S., in Europe, and in Latin America.

The paper proceeds as follows: in Section 2 we present some key data facts on lockdowns and their economic effects in the U.S. and discuss the relevant literature. Section 3 discusses the model, including the novel policies, which are further elaborated in online Appendix A. Section 4 presents the calibration and the solution methodology. Section 5 presents the results. Section 6 explores the underlying mechanism. Section 7 examines the relation between the model planner solution and actual outcomes in two U.S. states – NYS and Florida. Section 8 concludes.

2 Background

We briefly present key facts pertinent to the current analysis and the relevant parts of the rapidly-growing literature in Economics on COVID19.

2.1 Key Data Facts

We present U.S. data facts focusing on the variables that play a key role in our analysis. We look at the entire U.S. and at the six biggest states, namely, California, Texas, Florida, New York, Pennsylvania, and Illinois, encompassing about 40% of the U.S. population. Panel a in Figure 1 shows data of a stringency index of lockdown restrictions and closures – school closings, workplace closings, public event cancellations, closure of public transportation, public information campaigns, internal movement restrictions, and international travel controls – computed by the Blavatnik School of Government at the University of Oxford. The figure shows the index, in 14-days MA terms, from late January to December 2020; see the methodology in Hale et al (2020).

Figure 1: Background data

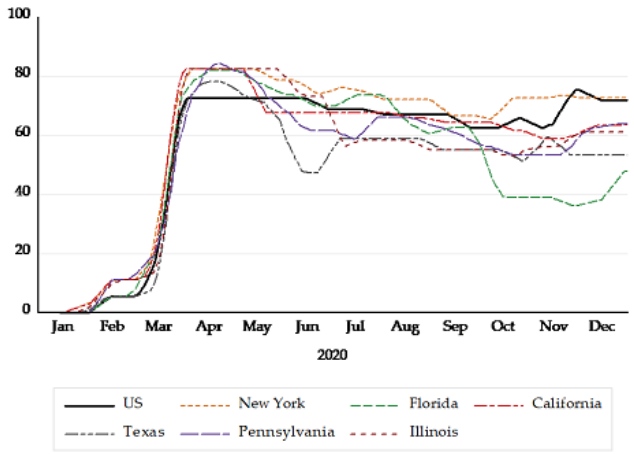

a. Oxford Stringency Index Across U.S. States in 2020, 14 days moving average

Source: Oxford Coronavirus Government Response Tracker, https://github.com/OxCGRT/covid-policy-tracker

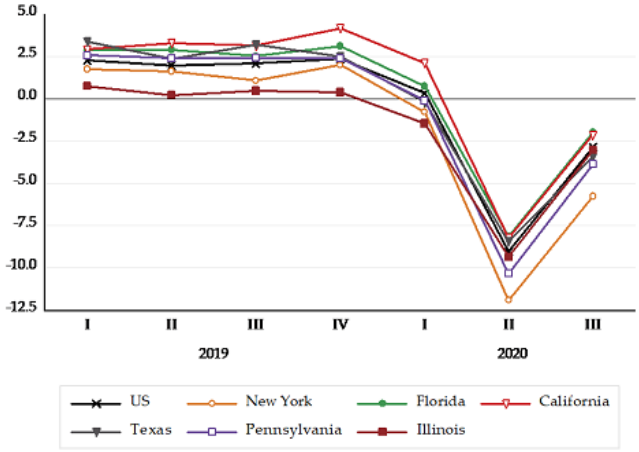

b. GDP Growth Across U.S. States 2019-2020, $Q_t/Q_{t-4} - 1$ (%)

Source: Gross Domestic Product by State, Bureau of Economic Analysis https://www.bea.gov/data/gdp/gdp-state.

Figure 1 (continued)

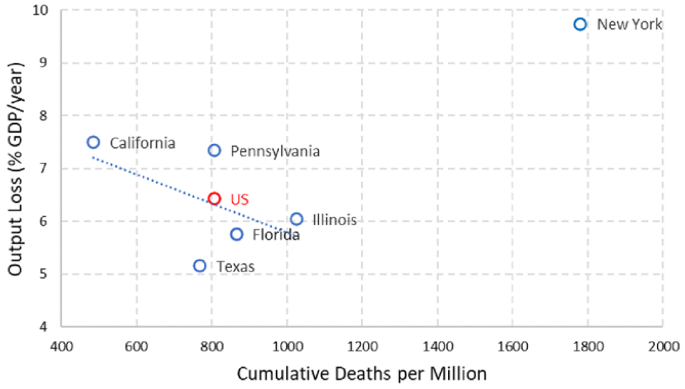

c. 2020 GDP Loss and COVID 19 Deaths in U.S. States

Source: State-level employment from CES, Bureau of Labor Statistics (www.bls.gov); cumulative death count from the COVID-19 Data Repository, Center for Systems Science and Engineering (CSSE) at Johns Hopkins University (https://github.com/CSSEGISandData/COVID-19); and authors' computations (see Appendix B for full description of the computation procedure)

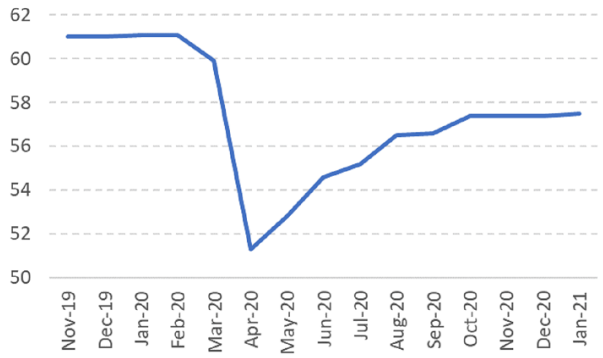

d. Employment to Population Ratio in the U.S. in 2020

Source: FRED

The emerging pattern shown by the figure is that following a lag in response after the February outbreaks, there was a fast rise in lockdown measures in March 2020. Subsequently policy became more heterogenous and more volatile across states and over time.

We briefly summarize the main points which can be seen in the figure: in NYS there was stability of measures over a few weeks, very gradual release from May, and some re-tightening from late September. California had a broadly similar response, but release was less gradual, policy became looser, and it re-tightened later, relative to NYS. Pennsylvania can be described in similar terms to California but went even looser. Illinois kept the tightest measures longer, till late May, but then came down faster and looser than the aforementioned states. It re-tightened in October but remained much looser than NYS. Very different behavior was shown by the other two states: Texas did not stay tight long, came down fast to a much lower level of restrictions, and tightened somewhat from July. Florida did stay with tight restrictions longer than Texas, but then went on a long release period, from April to October, achieving the lowest restrictions relative to the other five states, doing some re-tightening only in December.

Overall, the tightest restrictions were imposed in New York State and the most loose in Florida. In terms of the index, the latter's stringency was 55% of the former in November. Standard deviations of the index over the entire period are high, with a coefficient of variation of 0.4 to 0.5.

Panel b in Figure 1 shows GDP growth for the same states in 2019 and 2020. The figure shows GDP growth measured in terms of the current quarter relative to the same quarter in the preceding year. In 2019 these rates for the entire U.S. ranged roughly between 2% and 2.3%. In 2020 these rates were 0.3%, -9%, and -2.8% in the first three quarters, respectively. In terms of the states, four states had negative growth already in Q1; by Q2 all were in decline, with rates ranging from -8% to -12%; in Q3 this decline softened to a range of -2% to -6%.

Panel c in Figure 1 puts together data on deaths and output loss in the period March to November 2020. Output loss is imputed on the basis of actual employment data in 2020 and counterfactual employment projections for 2020. The details of the imputation procedure are described in Online Appendix B. The main feature of panel c is the very diverse experience of the different states. First, within the group of states excluding New York State, there seems to be a trade-off between output loss and cumulative death (see the dotted, linear line in the figure). This trade-off is broadly consistent with the interventions stringency dynamics presented in panel a of Figure 1, with states that had short-lived or less stringent measures losing less output but faring worse in terms of the death toll. The states are not perfectly aligned on the line, reflecting background variation across locations in terms of population density, healthcare quality, age composition, occupational composition, propensity to comply with restrictions, and numerous other factors. Second, the experience of New York State is strikingly different, dwarfing the outcomes in the other states on both dimensions. Our analysis sheds light on how such different results arise, deriving the outcomes depicted on the figure axes as endogenous variables.

We show that the diversity of scenarios depend on the available policy instruments and on the properties of the disease and the economy. We also show how outcomes can improve significantly when the timing of the interventions is set optimally, and particularly so when using the cyclical policy instruments, that are at the focal point of our normative analysis.

2.2 The Literature

There has been an explosion of research in Economics on COVID19. Reviews and discussions are provided by Avery, Bossert, Clark, Ellison, and Ellison (2020) and Baqaee, Farhi, Mina, and Stock (2020). Two kinds of papers are relevant for the current analysis.

One is work using the concept of an optimizing planner. It examines the health-related losses due to the pandemic in economic terms and the economic consequences of public health policy. An objective function is defined, with values taking into account output losses and the value of statistical life. Thus, tradeoffs are measured and alternative policies are evaluated. The planner constraints include, inter alia, disease dynamics typically examined within the SIR epidemiological model. Prominent contributions include Abel and Panageas (2020), Acemoglu, Chernozhukov, Werning, and Whinston (2020), Alvarez, Argente, and Lippi (2020), Farboodi, Jarosch, and Shimer (2020), and Jones, Philippon, and Venkateswaran (2020).

The second kind of work includes papers which tie macroeconomic dynamics to the epidemiological dynamics of the SIR model. These models posit that individual rational economic behavior has two-way connections with disease transmission. Notable contributions include Atkeson, Kopecky, and Zha (2021), Eichenbaum, Rebelo, and Trabandt (2020), Garibaldi, Moen, and Pissarides (2020), and Krueger, Uhlig, and Xie (2020). An elaborate analysis, emphasizing heterogeneous agents, is offered by Kaplan, Moll, and Violnate (2020) using the SIRD model.

It should be noted that in the epidemiological literature, pandemic or epidemic management is a key topic of study. Inter alia, it deals with the measurement of key parameters needed for policy, such as the reproduction parameter, which are also at the focus of the current paper. Prominent examples of such studies, pre-COVID 19, include Mills, Robins, and Lipsitch (2004) and Wallinga, van Boven, and Lipsitch (2010).

3 The Model

We model an optimizing social planner who operates within a SEIR model of the epidemic and a model of the macroeconomy. We elaborate on the novel policy strategies based on time restrictions.

3.1 The Evolution of the Epidemic

We analyze the evolution of the epidemic in two complementary blocks – infection transmission and clinical progression.

The infections transmission block is characterized by the SEIR Erlang model, reflecting the epidemiological properties of COVID19.[1] Before contacting the disease for the first time, a person is Susceptible (S). Once a person gets infected, disease progression is split into distinct compartments – Exposed (E), Infectious (I), and Resolved (R). We denote by β the infections transmission rate, σ, the transition rate from E to I, and γ, the transition rate from I to R. An infected individual spends some time in each compartment before moving on to the next one. The person is infectious only when in the I compartment, but not when residing in the preceding E compartment. The time durations spent in the E and I compartments are known as the latent and infectious periods, respectively. Once people move to the Resolved stage, they no longer participate in disease transmission. With Poisson transition rates between compartments, the residence times in each of them are distributed exponentially, and thus have zero mode. Exponential distributions capture the mean but not the mode of the biologically accurate distributions of residence times, because in reality what most people spend in each stage is close to the mean of the distribution, rather than zero. Therefore, we split the E and I compartments into two sub-compartments and double the rate of transition. Now, the latent and infectious periods are the sum of the time spent in the E_1 and E_2 or I_1 and I_2 sub-compartments, respectively. Their distribution is the sum of exponentially distributed random variables, a special case of the Gamma distribution, known as the Erlang distribution. The means of Erlang distributions remain $1/\sigma$ and $1/\gamma$, but the modes are now near the means, as they should be. In the remainder of the paper we shall refer to this model as the $SEIR$ model, without noting the number of sub-compartments.

Graphically, this block is presented in panel a of Figure 2.

[1] The model is essentially based on the seminal contribution of Kermack and McKendrick (1927). Its present form is discussed in Champredon, Dushoff, and Earn (2018). See Bar-On, Baron, Cornfeld, Milo and Yashiv (2021) for a more detailed analysis, where we explain the need for the two complementary model blocs.

Figure 2: The Model

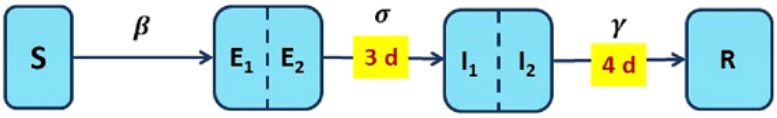

a. The SEIR-Erlang block

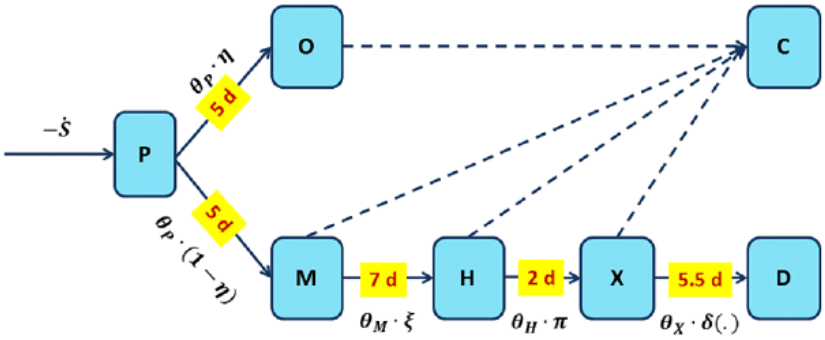

b. The Clinical block

The following equations describe this block. Throughout, all stock variables are expressed as a fraction of the population.

$$\begin{aligned}
\dot{S}(t) &= -\beta(t) \cdot (I_1(t) + I_2(t)) \cdot S(t) && (1)\\
\dot{E}_1(t) &= \beta(t) \cdot (I_1(t) + I_2(t)) \cdot S(t) - 2\sigma E_1(t) && (2)\\
\dot{E}_2(t) &= 2\sigma E_1(t) - 2\sigma E_2(t) && (3)\\
\dot{I}_1(t) &= 2\sigma E_2(t) - 2\gamma I_1(t) && (4)\\
\dot{I}_2(t) &= 2\gamma I_1(t) - 2\gamma I_2(t) && (5)\\
\dot{R}(t) &= 2\gamma I_2(t) && (6)
\end{aligned}$$

An important parameter is the reproduction number $\mathcal{R}_t$, which is the average number of people infected by a person, and is given by:

$$\mathcal{R}_t = \frac{\beta(t)}{\gamma} \tag{7}$$

We use $\mathcal{R}_t$ for the reproduction number at date t and denote the basic reproduction number by $\mathcal{R}_0$ at the initial stage, when $S(0) = 1$. Beyond the initial $t = 0$, our formulation will allow for $\mathcal{R}_t$ to be affected by policy and by rational individual behavior, as elaborated below in sub-section 4.1. We shall also be discussing the effective reproduction number, defined as:

$$\mathcal{R}_e = S(t)\mathcal{R}_t \tag{8}$$

The clinical block describes the clinical progression of the disease and the progression of new cases through the healthcare system, depending on the development and severity of symptoms. We postulate the following. Once infected, a person enters an incubation period, a P state, during which there are no symptoms, lasting for $1/\theta_P$ on average. Following it, a person either remains asymptomatic (O) or develops symptoms (M). Denote the share of asymptomatic cases by η. The others $(1 - \eta)$ develop symptoms, and with probability ξ are hospitalized (H). A given share π of patients become critically ill (denoted X), i.e., develop conditions requiring transition to ICU. Once critically ill, a fraction $\delta(\cdot)$ dies. We specify the death probability, once critically ill, as:

$$\delta(X(t), \overline{X}) = \delta_1 + \delta_2 \cdot \frac{\mathbf{I}(X(t) > \overline{X}) \cdot \left(X(t) - \overline{X}\right)}{X(t)} \tag{9}$$

where $\overline{X}$ denotes ICU capacity and $\mathbf{I}$ is the indicator function.

At any stage, a person may recover (C). The clinical block is represented graphically in panel b of Figure 2.

The analytical description of the symptomatic branch is:

$$\dot{P}(t) = \beta(t) \cdot (I_1(t) + I_2(t)) \cdot S(t) - \theta_P \cdot P(t) \quad (10)$$

$$\dot{M}(t) = (1-\eta) \cdot \theta_P \cdot P(t) - \theta_M \cdot M(t) \quad (11)$$

$$\dot{H}(t) = \xi \cdot \theta_M \cdot M(t) - \theta_H \cdot H(t) \quad (12)$$

$$\dot{X}(t) = \pi \cdot \theta_H \cdot H(t) - \theta_X \cdot X(t) \quad (13)$$

$$\dot{D}(t) = \delta(X(t)) \cdot \theta_X \cdot X(t) \quad (14)$$

The parameters $\theta_P, \theta_M, \theta_H$, and θ_X relate to the average time that passes between the stages of infection, symptoms onset, hospitalization, ICU admission, and death, respectively.

3.2 The Economy

The economy is described as follows. We use a linear production technology:

$$Y(t) = AN(t) \quad (15)$$

where A is technology and other inputs and $N(t)$ is employment. We normalize steady state output to unity:

$$Y^{SS} = 1$$

During COVID 19 we posit that the number of people who can work daily, $N(t)$, is reduced relative to the steady-state level N^{SS} and is given by:

$$N(t) = N^{SS} \cdot \rho \cdot (1 - D(t) - X(t) - H(t) - \phi M(t)) \quad (16)$$

where $0 < \rho \leq 1$ is the fraction able to work given current policy restrictions, and $0 \leq \phi \leq 1$ is the fraction of people with symptoms who do not work. If $\phi = 1$, anyone who develops symptoms self-isolates immediately and does not work.

In the planner problem below, the flow loss of output is thus given by:

$$1 - \frac{N(t)}{N^{SS}} = 1 - \rho \cdot (1 - D(t) - X(t) - H(t) - \phi M(t))$$

3.3 Policy Based on Time Restrictions

The novel policy, pertaining to the entire population, was introduced in Karin et al (2020), where its epidemiological implications are analyzed extensively. Following an initial lockdown, move to a regime of k days of work and $14 - k$ days of lockdown, every 14 days. On work days, people are released from lockdown with strict hygiene and physical distancing measures on the same k weekdays for everyone. On lockdown days, people are kept away from work places as well as from other public spaces. Epidemiological measures need to be used throughout, including rapid testing, contact isolation, and compartmentalization of workplaces. Table 1 offers a visual summary.[2]

[2] All strategies respect regular weekends, facilitating application.

Table 1: Menu of the Cyclical Strategies

k	Strategy	Workdays locked			week 1							week 2						
		week 1	week 2	in total	M	T	W	T	F	S	S	M	T	W	T	F	S	S
0	lockdown only	5	5	10														
3	3-11	2	5	7														
4	4-10	1	5	6														
5	week on, week off	0	5	5														
6	3-day week	2	2	4														
7	7-7	1	2	3														
8	long weekend	1	1	2														
14	no intervention	0	0	0														

Locked Open

Note:
k is the number of open (non-lockdown) days every 14 days.

Epidemic dynamics using these policies are discussed in detail below, where they are depicted graphically in Figures 4 and 5 (see Section 5).

The rationale for the policy is as follows. Cyclical strategies reduce the average value of the reproduction parameter – which will be shown below to capture the progress of the disease – through two effects: time-restrictions and anti-phasing.

The *time-restrictions effect* is a reduction in the time T that an infectious person is in contact with many others, compared to the situation with no lockdown. For example, a 4-day work, 10-day lockdown cycle ($k = 4$) reduces T to $\frac{4}{14}T \approx 0.3T$. The *anti-phasing effect* uses the timescales of the virus against itself. Most infected people are close to peak infectiousness for about 3-5 days, beginning after a latent period of about 3 days (on average) after exposure. A proper work-lockdown cycle, such as a 4-work 10-lockdown schedule, allows most of those infected during work days to reach maximal infectiousness during lockdown, thus avoid infecting many others. Those with significant symptoms can be infectious for longer, but remain hospitalized, isolated, or quarantined along with their household members, preventing secondary infections outside the household.

As Table 1 shows, we only consider $k \leq 8$ in our analysis of the cyclical strategies. This is because higher values of k imply shorter periods of lockdowns, for example, locking only on weekends. Though similar lockdown policies have been implemented (for example, in India), they do not line up with the epidemiological rationale of the cyclical policies. Furthermore, we find that, in the U.S. context, such extremely open policy tools are hardly consistent with a policy of efficient epidemic suppression.

Online Appendix A provides further details.

3.4 The Planner Loss Function

The planner is concerned by output loss and by loss of life. The former loss is due to employment falling below steady state levels due to lockdowns. The latter loss is due to deaths generated by the epidemic, which depend on ICU capacity. The problem is thus formulated as follows:

$$\min_{T_0,T_1,T_2} V = \int_{T_V=0}^{\infty} f(T_V) \cdot \left(\int_0^{T_V} e^{-rt} \cdot \left(\frac{Y^{SS}}{N^{SS}} \cdot \left(N^{SS} - N(t) \right) + \chi \cdot Y^{SS} \cdot \dot{D}(t) \right) dt + R_D(T_V) + R_Y(T_V) \right) \tag{17}$$

subject to equations (1)-(16).

The loss function V is minimized in PDV terms (r is the discount rate) over the infinite horizon. The loss function includes both lost (steady state) output per worker $\frac{Y^{SS}}{N^{SS}}$, due to a decline in employment $N(t)$ relative to steady state N^{SS}, [3]and the value (with parameter χ) of lost life, where $\dot{D}(t)$ denotes fatalities flow as a fraction of the population. The parameter χ reflects estimates of

[3]As we have assumed a linear production functon, $\frac{Y^{SS}}{N^{SS}} = \frac{Y(t)}{N(t)}$.

the Value of Statistical Life in steady state output per capita terms and is defined and discussed in sub-section 4.2 below. The term of lost life is affected by the breach of ICU (see equations (9) and (14)). The expression $f(T_V)$ denotes the probability distribution function of the availability of a vaccine at time T_V. We assume that following vaccine arrival, the pool of susceptibles drops to zero, so that the epidemic stops growing. Given each cyclical strategy k, the planner chooses the optimal intervention timing: T_0 lockdown of the economy; T_1 implementation of a cyclical strategy; T_2 release of the economy. It is important to note that we constrain the planner possibilities here for tractability. The benefits of the cyclical policy tools that we are thus able to find are likely to mark a lower bound of their true advantage over real-world strategies. Note, too, that when we introduce benchmark policies below, in those we shall not constrain the planner in a similar way.

After time T_V, there is a residual cost due to death toll $R_D(T_V)$ and output loss $R_Y(T_V)$, which accompany the decline of the epidemic. These terms are defined as follows:

$$\frac{R_D(T_V)}{Y^{SS}} = \chi \cdot \underbrace{\delta_1 \cdot (X(T_V) + \pi \cdot H(T_V) \cdot \xi \cdot ((M(T_V) + (1-\eta) \cdot P(T_V))))}_{\text{the expected number of people who will die after } T_V} \cdot e^{-rT_V} \tag{18}$$

$$\begin{aligned} \frac{R_Y(T_V)}{Y^{SS}} = & \underbrace{\phi \cdot (M(T_V) + (1-\eta) \cdot P(T_V))}_{\substack{\text{the expected number of people not able to work} \\ \text{out of symptomatic}}} \cdot \int_{T_V}^{T_V + \frac{1}{\theta_M}} e^{-rt} dt + \\ & \underbrace{(H(T_V) + \xi \cdot (M(T_V) + (1-\eta) \cdot P(T_V)))}_{\text{the expected number of people who will be hospitalized after } T_V} \cdot \int_{T_V}^{T_V + \frac{1}{\theta_H}} e^{-rt} dt + \\ & \underbrace{(X(T_V) + \pi \cdot (H(T_V) + \xi \cdot (M(T_V) + (1-\eta) \cdot P(T_V))))}_{\text{the expected number of people who will be in ICU after } T_V} \cdot \int_{T_V}^{T_V + \frac{1}{\theta_X}} e^{-rt} dt + \\ & \underbrace{\delta_1 \cdot (X(T_V) + \pi \cdot (H(T_V) + \xi \cdot ((M(T_V) + (1-\eta) \cdot P(T_V)))))}_{\text{the expected number of people who will die after } T_V} \cdot \int_{T_V}^{\infty} e^{-rt} dt \end{aligned} \tag{19}$$

3.5 Modelling Vaccine Arrival Time

We avoid modelling an arrival time known with certainty because it can create an artefact in the optimal plan. The planner may enable an outbreak shortly before vaccine arrival, relying on the vaccine to eradicate it. Such a plan is not robust to delays in the arrival time. We also avoid modelling it using a Poisson

process since exponential distribution has a mode of zero which is implausible in case of vaccine development.

Rather, we assume that the arrival of the vaccine is a result of simultaneous competition among many firms. The time of arrival is the minimum development time across these firms.[4] The distribution of arrival time is then well approximated by a Gumbel distribution (see Kotz and Nadarajah (2000)), which is a member of the family of extreme value distributions. Specifically, it is used for modeling the minimum of a sample from many distributions, including exponential, logistic, and normal distributions. Under mild regularity conditions, it is suitable to be a model for a sample minimum even when the distributions from which the sample is drawn are unknown. In our setting, we remain agnostic about the distributions of vaccine development time by individual firms.

The cumulative distribution function $G(x)$ of a Gumbel distribution is defined over the real numbers and parametrized by a location parameter μ_G and a scale parameter σ_G :

$$G(x;\mu_G,\sigma_G) = 1 - \exp\left(-\exp\left(\frac{x-\mu_G}{\sigma_G}\right)\right) \tag{20}$$

We anchor the distribution's parameters (μ_G, σ_G), by positing that the mean of the distribution is 540 days, and that the probability of such vaccination before day 360 is only 1%. These assumptions engender two linear equations:

$$\begin{aligned} E(Gumbel\,(\mu_G,\sigma_G)) &= \mu_G - EulerGamma\cdot\sigma_G = 540 \\ Q(Gumbel\,(\mu_G,\sigma_G),q) &= \mu_G + \log\left(-\log\left(1-q\right)\right)\cdot\sigma_G = 360 \end{aligned}$$

where E is the mean and Q is the quantile function. Targeting a mean of 540 and $Q(q = 0.01) = 360$ leads to the solution of $\mu_G = 565.83, \sigma_G = 44.74$.

We make these assumptions given the progress actually made in 2020 and the start of vaccination in December 2020. In terms of the model, T_V refers to the time of sufficient vaccination; with logistics, production times, gradual take-up rates, etc. an expected 540 days seems reasonable at the time of writing (March 2021). For the U.S., given the initial outbreak took place at some point in February 2020, this means an arrival time in August 2021. This number (540 days) is also the one used by Alvarez et al. (2020) and Shimer et al. (2020) and is the middle of the range in Acemoglu et al. (2020).

3.6 Benchmarks

We shall compare the results of simulating the model, calibrated to the U.S. economy, to the following benchmarks:

(i) and (ii) The polar cases of no policy intervention (i.e., no lockdown) or full lockdown till vaccine arrival.

[4] At the time of writing, March 2021, three vaccines have actually been approved by the FDA in the U.S., two are close to approval, over 80 vaccines are in clinical trials, and over 180 are in pre-clinical evaluations. See https://www.who.int/publications/m/item/draft-landscape-of-covid-19-candidate-vaccines

(iii) Optimal lockdown; this is essentially the case of $k = 0$.

(iv) A theoretical path trying to mimic real-world policy by re-interpreting the planner problem as choosing thresholds for lockdown policy in terms of the critically ill, X. The first threshold defines a level X_0 whereby if $X_t > X_0$ an initial lockdown is imposed. Subsequently, a second threshold defines a level X_1 whereby if $X_t < X_1$ lockdown is released. Finally, a third threshold defines a level X_2 whereby if $X_t > X_2$ lockdown is re-imposed. The planner chooses the three thresholds optimally. Note that this strategy leads to recurrent lockdown and release policies, and, that the planner here is not as constrained as in the case of the cyclical strategies, when we allowed for only three optimal points in time to be chosen.

In Section 7 we compare the model to the actual experience of the states of New York and Florida.

4 Calibration and Solution Methodology

At first, we calibrate the model to fit the U.S. economy, which – as seen in Section 2 above – was badly hit by COVID19. Throughout we work in daily terms. In Section 7, we shall discuss the methodology and calibration values used for the analysis of two specific states in the U.S.

4.1 Calibration of the Epidemiological Model

In Table 2, we present the relevant parameter values for the two blocks, where we rely on sources in the epidemiological and medical literatures published in Science, Nature, the Lancet, and JAMA, as detailed in the table's notes.

Table 2: Calibration

	Interpretation	Range	Parameter value
a. The Infection Transmission Block (SEIR)			
σ	latent period duration	$3-5$ days	$1/3$
γ	infectious period duration	$4-5$ days	$1/4$
b. The Clinical Block			
θ_P	incubation period	$5-6$ days	$1/5$
θ_M	days from symptoms till hospitalization	7 days	$1/7$
θ_H	days in hospital till ICU	2 days	$1/2$
θ_X	days in ICU before death	5.5 days	$1/5.5$
η	Prob. to be asymptomatic	$20\%-50\%$	0.5
ξ	Prob.of hospitalization when symptomatic	$\frac{\#Hospitalized}{\#Infected} = [2\%-4\%]$	$\frac{0.04}{1-0.5} = 0.08$
π	Prob. of ICU admission	$10\%-40\%$	0.4
IFR	Infection Fatality Rate (implied)		0.008

Sources:

1. Panel a: Bar-On et al (2020); He at al (2020); Li et al (2020); Tian et al (2020);

2. Panel b – Bar-On et al (2020); Huang et al (2020); Richardson et al (2020); Salje et al (2020).

Notes:

1. $\frac{\#Hospitalized}{\#Infected} = \frac{\#Hospitalized}{\#Symptomatic} \cdot \frac{\#Symptomatic}{\#Infected} = \xi \cdot (1-\eta) \implies \xi = \frac{\frac{\#Hospitalized}{\#Infected}}{1-\eta}$;

2. $IFR = (1-\eta) \cdot \xi \cdot \pi \cdot \delta_1$. We use $\delta_1 = 0.5$.

We use $\overline{X} = \frac{58{,}094}{329.529*10^6} = 1.8 \times 10^{-4}$ based on an estimate of 58,094 ICU beds by the Harvard Global Health Institute.[5] The implied Infection Fatality Rate (IFR) is 0.8%,[6] consistent with the recent estimates for the U.S. by the IHME COVID-19 Forecasting Team (2021).

The path assumed for the reproduction parameter merits discussion. The idea is to model a time-varying parameter, $\mathcal{R}_t$. The reason is that $\mathcal{R}_t$ reflects both rational individual behavior and the effects of suppression policy. We take into account that individuals adjust to the new environment and behave differently, both with and without government interventions.[7] In particular, as the epidemic unfolds, people become increasingly aware of the risks and adjust their behavior. This adjustment is manifested in avoiding or reducing social contact and taking precautions, such as wearing masks. These changes happen in part as a direct result of government NPIs and in part as a voluntary response. It is a rational choice to adopt new norms of behavior, even when restrictions by the government are weakened or removed. As a result, the speed of disease transmission declines relative to its start.

The way we proceed is to model the time variation in $\mathcal{R}_t$ by relying on data estimates as follows.

(i) Initial level. We set

$$\mathcal{R}_0 = 2.50 \tag{21}$$

We get the value of 2.50 in equation (21) using the methodology of Fernandez-Villaverde and Jones (2020), adapted to our model[8], and daily death flow data taken from Johns Hopkins University CSSE (2020). This yields estimates of $\mathcal{R}_0$ values of 2.67 on March 17, 2020 and 2.48 on March 18, 2020. This is the reproduction number during the initial phase of the epidemic, before significant lockdowns were imposed in the U.S. [9]

(ii) Subsequent values. To reflect the fact that over the course of the initial outbreak and following it, individuals change their modes of behavior and economic activity, including compliance with NPIs, we allow the reproduction number in subsequent periods to be lower than the initial $\mathcal{R}_0$. We posit that there is a value of $\mathcal{R}_t$ during times of lockdown, to be denoted $\mathcal{R}_L$, and another value at other times, denoted $\mathcal{R}_W$ ("work"). Both are lower than $\mathcal{R}_0$ to take into account the fact that individuals have adjusted to the new environment and are taking more precautions. When lockdowns are in place, policy and individual responses together engender $\mathcal{R}_L < \mathcal{R}_W$.

For their calibration, we rely on two sets of estimates.

[5] See https://globalepidemics.org/our-data/hospital-capacity/

[6] This rate is given by $IFR = \xi \cdot \pi \cdot (1 - \eta) \cdot \delta_1$

[7] These mechanisms are explored in the second strand of literature discussed in sub-section 2.2 above.

[8] See online Appendix C for details.

[9] As noted by Farboodi et al. (2020), social activity and population mobility started declining even before that. Therefore, it is conceivable that prior to mid March the reproduction number was even higher. However, due to very incomplete and noisy data on early COVID19 fatalities it is not possible to credibly infer the reproduction number in the US before mid March (see, for example, the very wide confidence intervals in Li et al., 2020)

First, Karin et al (2020) review the literature and estimate values for $\mathcal{R}_L$ and $\mathcal{R}_W$.[10] These relate to developed countries with a population density of over 100 people per square km. Figure 3 reports their estimates.

Figure 3: Estimates of $\mathcal{R}_W$ and $\mathcal{R}_L$

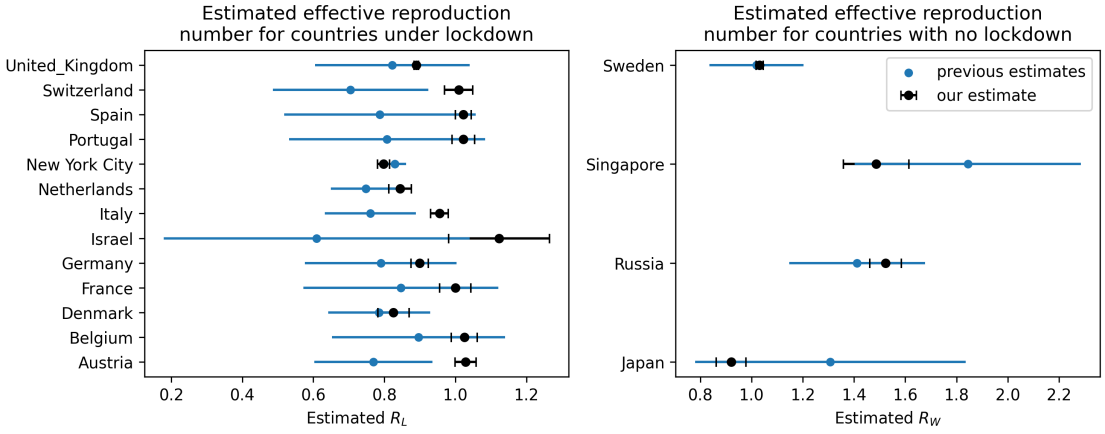

Source: Karin et al (2020).

[10]The full details of their analysis, including references and the code, are found at: www.github.com/milo-lab/

Looking at the black points in the figure, the value of 1.50 for $\mathcal{R}_W$ is the upper bound of estimates; the estimates for $\mathcal{R}_L$ range from 0.6 to 0.9 with a value of 0.80 as the estimate for NYC.

Second, we use the U.S. estimates of Fernandez-Villaverde and Jones (2020) for the biggest 15 states in the U.S., covering 65% of the U.S. population[11] We look at the minimal and maximal values of the estimated $\mathcal{R}_t$ series from April 1, 2020 till September 30, 2020. According to the Oxford Stringency Index, discussed in sub-section 2.1 above, this period covers lockdowns and release in all of the states, at different points in time. These $\mathcal{R}_t$ values are indicative of $\mathcal{R}_L$ and $\mathcal{R}_W$: $\mathcal{R}_L$ cannot be lower than the minimal data value, and $\mathcal{R}_W$ cannot be higher than the maximal data value. The median (average) minimal value across the 15 states is 0.68 (0.61) and the median (average) maximal value across the 15 states is 1.42 (1.49).

Given these two sets of estimates we posit values that are conservative, in the sense of being biased against the cyclical strategies, i.e., $\mathcal{R}_L$ and $\mathcal{R}_W$ that are relatively high:

$$\mathcal{R}_t = \begin{Bmatrix} 1.50 & \mathcal{R}_W, work \\ 0.80 & \mathcal{R}_L, lockdown \end{Bmatrix} \tag{22}$$

(iii) Dynamics of the reproduction parameter. To capture the gradual nature of learning and adjustment of individual behavior, we posit that a certain minimal time should pass under lockdown before the reproduction number declines from its initial value $\mathcal{R}_0$ to $\mathcal{R}_W$. To capture this time span, we look at two sources.

a. Using the Fernandez-Villaverde and Jones (2020) methodology applied to our model, as discussed in online Appendix C, we get that it takes 8 days to get from $\mathcal{R}_t = 2.48$ to $\mathcal{R}_t = 1.50$. This decline took place in the third week of March, when lockdowns only started to unfold. Thus, we interpret this decline mainly as rational adjustment of behavior.

b. We use Imperial College COVID-19 Response Team (2020) estimates $\mathcal{R}_t$ for U.S. states since the start of the epidemic. We focus on the initial decline of $\mathcal{R}_t$ when suppression measures have been undertaken across the US and assume a log-linear decay function[12]

$$\ln \mathcal{R}(T_1^s) = \ln \mathcal{R}(T_0^s) - \widehat{\alpha}_s^{\log -linear} \cdot (T_1^s - T_0^s) \tag{23}$$

$$\widehat{\alpha}^{\log -linear} = \frac{\sum_{1}^{45} \alpha_s^{\log -linear}}{S} \tag{24}$$

We obtain two alternative estimates for the average speed $\widehat{\alpha}^{\log -linear}$ of a $\mathcal{R}_t$ decline, depending on the definition of the decline in period T_0^s to T_1^s:

[11]Due to insuffiicent estimates, we exclude the state of New Jersey. As noted, these authors infer $\mathcal{R}_t$ from daily death flow data taken from Johns Hopkins University CSSE (2020).

[12]Out of the fifty states and DC, six were not included in this analysis (AK, HI, MT, ND, SD, WY) because their initial values of the reproduction number were already below unity at the start of the epidemic.

a. The speed $\widehat{\alpha}^{\log-linear} = 0.027$ per day was obtained when $T_0^s =$ the day of the first $\mathcal{R}_t$ observation in the state, and $T_1^s =$ end of the decline (i.e., the point where $\mathcal{R}_t$ is not statistically different from 1 at 5%). It thus takes $\frac{\ln(2.5)-\ln(1.5)}{0.027} = 19.2$ days to get from 2.50 to 1.50.

b. The speed $\widehat{\alpha}^{\log-linear} = 0.065$ per day was obtained when $T_0^s =$ the day the highest $\mathcal{R}_t$ observed in the state; T_1^s as in (a). It takes $\frac{\ln(2.5)-\ln(1.5)}{0.065} = 7.9$ days to get from 2.50 to 1.50.

The decay time of $\mathcal{R}_t$ is 8 days based on Fernandez-Villaverde and Jones (2020) national death data, or 8 or 19 days based on the state-level data, Imperial model estimates. Again, we adopt a conservative calibration and assume that 14 days must pass before $\mathcal{R}_t$ declines from 2.50 to 1.50.

When we examine two specific U.S. states in Section 7, we revisit the computation of $\mathcal{R}_t$.

4.2 Calibration of the Economic Model

Discounting. We posit a 4% annual discount rate for the planner ($r = 0.04$), converted to daily terms.

The value of ϕ. We assume that all symptomatic people who are not hospitalized (M) self-isolate and so do not work ($\phi = 1$).

The value of ρ. We use a number of sources to determine ρ, the fraction of people working out of $N^{SS}$when in lockdown.

a. Panel d in Figure 1 shows BLS data on the U.S. employment-population ratio. It implies the following for the most stringent lockdown, in April 2020:

$$\rho = \frac{N(t)}{N^{SS}} = \frac{0.513}{0.61} = 0.84$$

b. Studying remote work, Dingel and Neiman (2020) find that 37 percent of jobs in the United States can be performed entirely at home, with significant variation across cities and industries.

c. An Economic Policy Institute (EPI) analysis[13] puts essential workers at 55,217,845. February 2020 employment was 158,759,000; hence $\frac{55.2}{158.8} = 0.35$.

d. A McKinsey Global Institute analysis[14] of all 804 occupations tracked by the BLS (O*NET data) assign each one a vulnerability rating of low, medium, or high. Low-vulnerability jobs are the essential ones, require no physical proximity to others, or are likely to guarantee pay even if workers are furloughed. Medium-vulnerability jobs require workers to be in proximity to coworkers but not the public; shutdowns affect 30 to 50 percent of these jobs. High-vulnerability jobs are nonessential roles that involve exposure to the public; shutdowns affect 70 to 90 percent of these jobs. This analysis estimates that a nationwide shutdown could leave 44 million to 57 million jobs vulnerable.

[13]See https://www.epi.org/blog/who-are-essential-workers-a-comprehensive-look-at-their-wages-demographics-and-unionization-rates/

[14]See https://www.mckinsey.com/industries/public-sector/our-insights/covid-19-and-jobs-monitoring-the-us-impact-on-people-and-places

Note that this analysis covers both remote work and essential workers. Hence $\rho = 1 - \frac{44}{158.759} = 0.72$ to $\rho = 1 - \frac{57}{158.759} = 0.64$.

From this discussion a reasonable conjecture is that $\rho \in [0.65, 0.80]$; we take $\rho = 0.65$ at the baseline; this value is consistent with values used by Kaplan, Moll, and Violante (2020). Subsequently, we also examine the value $\rho = 0.75$.

Value of Statistical Life.

We compute the value of life as follows:

$$\chi = \frac{\text{expected years remaining} \cdot \text{value of statistical life per annum}}{\frac{Y^{SS}}{POP}} \tag{25}$$

where POP is the population. As is well known, there is a wide set of estimates for the Value of Statistical Life (VSL). Indeed, Hall, Jones, and Klenow (2020) state that estimates of the VSL per annum range from $\$100,000$ to $\$400,000$. Greenstone and Nigam (2020) work with Environmental Protection Agency estimates of \$11.5 million for the VSL for adults, in 2020 terms. This translates into approximately $\$250,000$ per annum.

Taking the maximal value of the cited range of estimates, using the pre-COVID 19 GDP per capita at $\$65,430$, and the fact that COVID 19 deceased have an expected average of 14.1 years of life remaining (Hall, Jones, and Klenow (2020)), this yields:

$$\chi = \frac{14.1 * 400,000}{65,430} = 14.1 * 6.11 = 86.15 \tag{26}$$

In what follows we use a rounded number, $\chi = 85$, in the baseline case.

For a robustness check, we examine the following. A widely used value for annual VSL in per capita terms ($\frac{\text{value of statistical life per annum}}{\frac{Y^{SS}}{POP}}$) is 4, which yields $\chi = 14.1 * 4 = 56.4$. As mentioned, Greenstone and Nigam (2020) use an EPA-based number, yielding $\chi = \frac{14.1*250,000}{65,430} = 14.1 * 3.82 = 53.86$, which is close. We round this up to 60, and explore the latter as an alternative in sub-section 6.2 below.

4.3 Solution Methodology

To derive an optimal policy under each cyclical intrument, we use a numerical solver in Mathematica (NDSolve, see Abell and Braselton (2016)).

We find the values of the control variables (T_0, T_1, T_2) that minimize the planner cost function in problem (17) by conducting a hierarchical search of the three-dimensional control variables space. The restriction $0 \leq T_0 \leq T_1 \leq T_2 \leq 730$ is enforced throughout the search. In order to avoid the cost of an exhaustive grid search at daily granularity, we start with a rough grid in which T_0, T_1, T_2 are multiples of 16 and then refine it repeatedly. For each triplet (T_0, T_1, T_2) on the current grid we solve the continuous time system of ODE describing the stocks $S(t), E_1(t), E_2(t), I_1(t), I_2(t), R(t)$ in the SEIR block as described by equations (1)-(6) and the continuous time system of ODE describing the stocks $P(t), M(t), H(t), X(t), D(t)$ in the clinical block (equations (10)-(14))

given the policy regimes defined by (T_0, T_1, T_2), according to the calibration of Table 2.

Note that the timing of interventions (T_0, T_1, T_2) and the number of open days (k) in the cyclical strategy under consideration define the periods of time in which specific reproduction numbers – $\mathcal{R}_0, \mathcal{R}_L$, and $\mathcal{R}_W$ – are applicable. Therefore, we solve the systems (1)-(6) and (10)-(14) separately for each time period, given its relevant reproduction number. The stocks of infectious, critically ill, etc. at the endpoint of each time period serve as initial values for the ODE system describing the dynamics during the subsequent time period.

We use the following steps:

(i) In the very first period, initial values are taken from an infection seed of 0.01% of the population (100 people per million). Within this seed, infectious and latent subcompartments are initialized so as to be consistent with an initial exponential growth rate of the disease; susceptibles $(S(t))$ form the rest of the pool. The clinical block of the epidemiological model is initialized to 0 at $t = 0$.

(ii) Using the solution of the ODE system, a set of interpolated functions[15]describing the dynamics of all stocks $S(t), E_1(t), E_2(t), I_1(t), I_2(t), R(t), P(t), M(t), H(t), X(t), D(t)$, we are able to evaluate the planner's objective (17), which is a function of these stocks (through the cumulative deaths stock $D(t)$ and the employment stock $N(t)$ as defined in (16)). We solve the system of ODE for each point (T_0, T_1, T_2) on the current grid and identify the one for which the minimum of the objective function is attained. We keep this point and all points that produce values of the objective function within 20% of the minimal value. From these, we select 16 points that best span the control variable space. This is done by starting with the set that contains only the minimum point. We then add to this set the point that is the geometrically farthest from the set, and then the point that is second-farthest, and so on, until 16 points are added to the set. If there are less than 16 points yielding the value of objective function within 20% of the minimal value in the current step, we keep all of them for the next step.

(iii) The selected 16 grid points are the basis for the grid to be examined in the next iteration of the minimization. We expand the base grid by adding more points such that each point (T_0, T_1, T_2) in the base grid is complemented by 125 grid points located uniformly around it in a three-dimensional space. The resulting grid is fed into the next iteration of the optimization procedure, as described above. The process is repeated until minimum granularity of 1 day is reached and the grid cannot be further refined. The optimum is the point (T_0, T_t, T_2) on this grid, which is the most fine we get, with the lowest value of the objective function.

(iv) Finally, we verify that the solution is robust to the initial values fed into the optimization, and numerically ascertain that the above hierarchical procedure yields solutions that are close to the optimum obtained using exhaustive search.

The no intervention and full lockdown cases ((i) and (ii) in sub-section 3.6) are solved similarly imposing $(T_0 = T_1 = T_2 = T_V)$ and $(T_0 = 0$ and $T_1 =$

[15]Interpolated functions are approximate functions which values are found by interpolation.

$T_2 = T_V$), respectively. Optimal lockdown (case (iii) in sub-section 3.6) is found by imposing the condition $T_1 = T_2$, and solving for (T_0, T_1, T_2), as above. Finally, when solving the solution for optimal thresholds, (case (iv) in sub-section 3.6), for the three continuous control variables (X_0, X_1, X_2), we find the optimal thresholds minimizing the planner cost by conducting an exhaustive hierarchical search of the control variables space, spanning the values from 0 to $\overline{X}$ over a logarithmic discrete grid.

5 Results

We present the results for the baseline calibration of $\rho = 0.65$, $\chi = 85$, and $IFR = 0.8\%$. In the next section we shall explore some variations in these values.

The optimizing planner chooses how long to wait till first lockdown (T_0), when to start implementing a cyclical strategy (T_1), and when to release completely (T_2), for each instrument, namely for each given k. Optimal timing is based on probability-weighted scenarios for vaccine arrival over the horizon of two years.[16] In the simulations, vaccine arrival is actually realized on day 540, at its arrival time in expectation using the afore-discussed Gumbel distribution.

We present the results for the four benchmarks discussed in sub-section 3.6 above and six values of the k strategies. Table 3 reports the planner's optimal timing T_0, T_1, T_2, the resulting values of cost, V (in annual PDV, GDP per annum terms evaluated over two years), decomposed into V_Y, the value of foregone output and V_D, the value of lost life, and the cumulative number of dead, per 1 million people. Figures 4 and 5 show the time evolution of $I + E$ and of X for six selected strategies: three benchmarks (no intervention, optimal lockdown only, and thresholds on X) and three cyclical strategies ($k = 4, 6, 8$).

[16] According to the vaccine arrival time distribution that we assume, the probability that it will take more than two years to introduce the vaccine is practically 0.

Table 3: Outcomes of the Different Policy Strategies - Baseline

$$\rho = 0.65, \chi = 85, IFR = 0.8\%$$

		T_0	T_1	T_2	V	V_Y	V_D	D (per 10^6)
Non-cyclical								
(i)	No Intervention	540	540	540	1.13	0.03	1.10	13,023
(ii)	Full lockdown	0	540	540	0.50	0.50	0.00	4
(iii)	$k = 0$	40	133	133	0.42	0.10	0.32	3,834
(iv)	Thresholds	*n.a.*	*n.a.*	*n.a.*	0.34	0.32	0.02	212
Cyclical								
(v)	$k = 3$	9	28	483	0.32	0.31	0.00	45
(vi)	$k = 4$	0	14	511	0.29	0.29	0.00	27
(vii)	$k = 5$	0	14	540	0.27	0.26	0.01	166
$(viii)$	$k = 6$	0	100	540	0.27	0.26	0.01	137
(ix)	$k = 7$	0	128	540	0.29	0.24	0.05	596
(x)	$k = 8$	31	63	388	0.28	0.10	0.19	2,258

Notes:

a. T_0 is the start day of lockdown, T_1 start day of the cyclical strategy, and T_2 the release day; the numbers in these columns indicate day number since the start of the epidemic. The assumption is that vaccine arrival happens on day 540.

b. The loss function is given by:

$$V = \int_0^{540} e^{-rt} \cdot \left(\underbrace{\frac{Y^{SS}}{N^{SS}}(N^{SS} - N(t))}_{\text{output loss}} + \underbrace{\chi \cdot Y^{SS} \cdot \dot{D}(t)}_{\text{value of lost life}} \right) dt + (R_D + R_Y)$$

$$V_Y = \int_0^{540} e^{-rt} \left(\frac{Y^{SS}}{N^{SS}}(N^{SS} - N(t)) \right) dt + R_Y$$

$$V_D = \int_0^{540} e^{-rt} \cdot \chi \cdot Y^{SS} \cdot \dot{D}(t) dt + R_D$$

where $R_Y = R_Y(540)$ and $R_D = R_D(540)$) reflect residual output and death costs incurred from the moment of vaccine arrival on day 540 and till day 731, as defined in the planner problem in Section 3.

c. D is the stock of the deceased as a fraction of the population.

Figure 4: $E + I$ in selected strategies

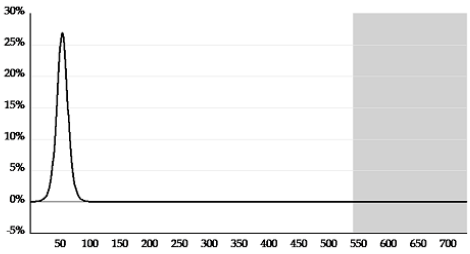

No Intervention

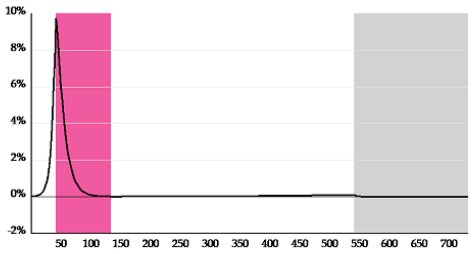

Lockdown only

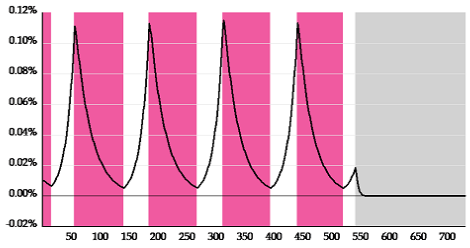

Thresholds

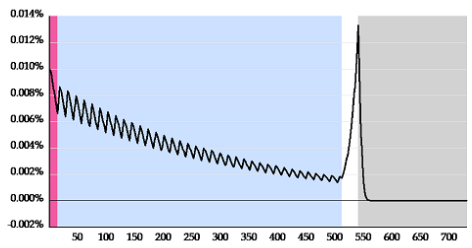

4-10

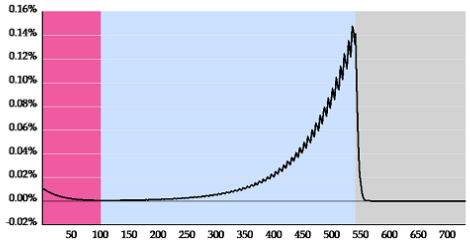

6-8

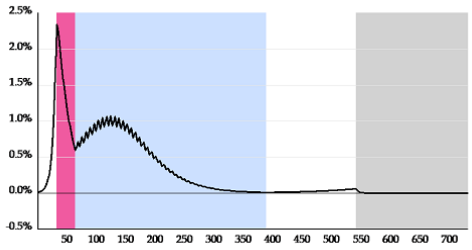

8-6

Figure 5: X in selected strategies

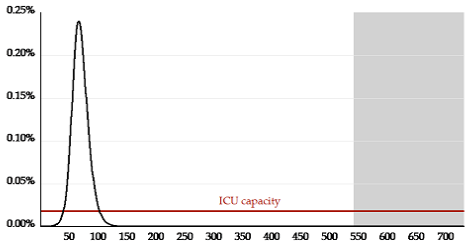

No Intervention

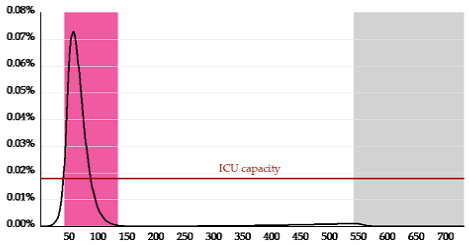

Lockdown only

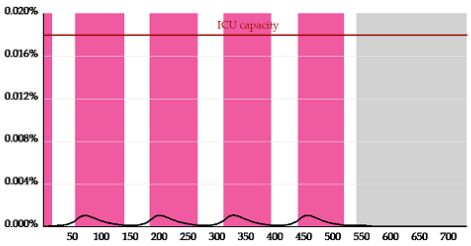

Thresholds

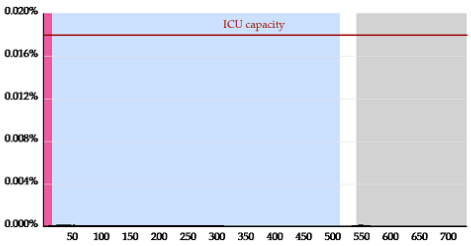

4-10

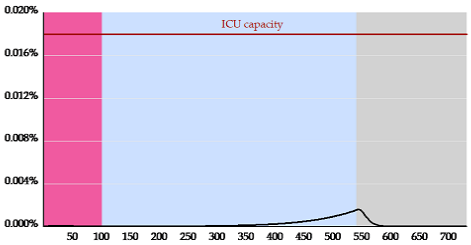

6-8

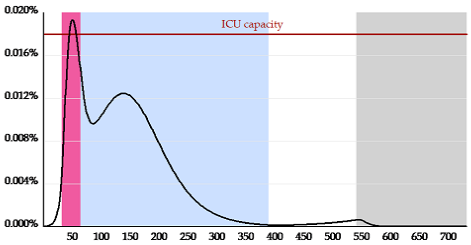

8-6

In the graphs, initial lockdown is marked by purple, the cyclical phase by blue, release by no color, and the post-vaccine arrival period by grey.[17]Table 3 and Figures 4 and 5 show that the results can be characterized as follows, discussing first the cyclical tools.

(i) *Cyclical strategies with low k* $(= 3, 4, 5, 6, 7)$ keep the epidemic under control and ICU capacity is not breached. For this case, the figures show the $k = 4$ and $k = 6$ strategies. In the infected $(E + I)$ figure 4 it can be seen that there is a rise in the number of infected over time but it remains extremely low. As can be seen in the X plot (figure 5), the number of critically ill is hardly apparent relative to the ICU constraint $\overline{X}$. This happens as k is relatively low and as the cyclical strategy is applied for a long time (blue region) following a quick initial lockdown (purple region). These strategies lead to relatively low numbers of deceased, between (approximately) $15,000$ and $200,000$, lower than the actual number of deceased in the U.S. by late September 2020. Total planner costs vary between 27% and 32% of annual GDP in PDV terms over two years, coming mostly from the value of foregone output.

(ii) *A cyclical strategy with high k* $(= 8)$ does not have the disease under control, as shown in the figures. There are two waves, whereby ICU capacity is breached in the first one. Note the scale of infection, which is much higher than in the preceding case. The initial lockdown (purple region) comes later, and the cyclical strategy (blue region) does not last as long. It leads to a relatively high number of deceased, approximately $750,000$. Total cost is 28% of annual GDP in PDV terms over two years, coming mostly from the value of lost life.

The results for the four benchmarks discussed in sub-section 3.6 above and reported in Table 3, to which we compare the afore-going cyclical policies, are as follows.[18] The first two are non-optimizing, extremal benchmarks.

(i) *The no intervention case* has the disease erupt, breach the ICU capacity constraint $\overline{X}$, and reach herd immunity (to be discussed in Section 6.1 below) at $S = 0.40$ by day 53, after which the epidemic starts to decline by itself. It leads to a high number of deceased – about 4.3 million people – and has a huge cost, at 113% of annual GDP in PDV terms over two years, most of it coming from the value of lost life (with $V = 1.13$ and $V_D = 1.10$).

(ii) *The full lockdown case* (not shown in the graphs) has the disease under control as it entails an immediate lockdown, remaining in place until vaccine arrival. It leads to a very low number of deceased, around $1,300$ people, and has a substantial cost, at 50% of annual GDP in PDV terms over two years, coming from the value of foregone output $(V = V_Y = 0.50)$.

(iii) *The case of optimal lockdown*, $(k = 0)$, marked "lockdown only" in the graphs, implies that a cyclical strategy is de facto unavailable to the planner and all the planner can do is optimally set the lockdown start and end dates. Un-

[17]Note that the graphs in Figures 4 and 5 have very different vertical scales, all in percent out of the population. In Figure 4, the range of the graph in the case of no intervention, is between 0% and 25% while that of the $k = 4$ strategy is between 0% and 0.01%. The scales of the other graphs are in between. In Figure 5 these ranges are 0% to 0.25% for no intervention and 0% to 0.018% for $k = 4$.

[18]While here we compare to theoretical benchmarks, note that in Section 7 below we directly compare the model results to two actual U.S. cases – New York State and Florida

like the full lockdown case, here the planner lets the epidemic erupt, breach the ICU capacity constraint $\overline{X}$, and only after 40 days locks for about three months. Subsequently the planner releases for good; disease growth is extremely slow, as the system gets close to herd immunity. The planner does not impose the lockdown for longer because its economic costs are too high. This strategy ends up with losses of 42% in annual GDP PDV terms, which is 8 percentage points lower than in the full lockdown, non-optimizing case. Most of this cost reduction comes from the gain in production, which more than compensates (in GDP terms) for the loss of value due to the substantial amount of deaths under this scenario, amounting to about 1.3 million fatalities.

(iv) *The thresholds policy case* follows the policy rationale adopted in many places in the real world; the planner optimally chooses thresholds for lockdown policy in terms of ICU hospitalizations, X. It keeps the epidemic under control and ICU capacity is not breached. In the figures one sees low rates of infection and a hardly discernible X series. The planner in this case is very cautious and locks the economy early, far ahead of the point of an immediate threat to ICU capacity. The disease develops in several consecutive waves that rise and fall as the planner switches between release and lockdowns. It leads to relatively low numbers of deceased, around $70,000$ people. Given that the U.S. has exceeded this number by early May 2020, it must be the case that U.S. policymakers have not been implementing this type of strategy optimally, or have been implementing some other policy altogether. Total cost in this benchmark case is 34% of annual GDP in PDV terms over two years, coming mostly from the value of foregone output (with $V = 0.34$, $V_Y = 0.32$).

Table 3 shows that the cyclical strategies entail much lower losses, as compared to the benchmark cases, varying between 27% and 32% in annual GDP, PDV terms.

6 Exploring Planner Policies

While the preceding section presented the baseline results, in this section we analyze their implications. First we study the underlying mechanism, exploring the rationale for the planner optimal decisions (sub-section 6.1). Second, we evaluate the cyclical policies by comparing them to the alternative benchmark policies using a plot of the policy frontier (6.2). Finally, we study variations in key parameters (6.3).

6.1 The Mechanism

To understand the underlying mechanism consider the following.

The progression of the epidemic can be classified according to the *effective* reproduction number $\mathcal{R}_e$ as follows:

(i) When $\mathcal{R}_e = 1$,[19] the population has reached herd immunity and an outbreak (i.e., a spurt of disease growth) is no longer possible, though susceptibles still do get infected.

(ii) Below that, when $\mathcal{R}_e < 1$, the epidemic is suppressed and the number of newly infected people declines with time.

(iii) When $1 \leq \mathcal{R}_e < 1.1$, the epidemic is slow growing; its doubling time is at least 6 weeks.

(iv) When $\mathcal{R}_e \geq 1.1$ there is an outbreak.[20]

Note that $\mathcal{R}_e$ depends both on the current reproduction number $\mathcal{R}_t$ and the current fraction of susceptibles $S(t)$, i.e., $\mathcal{R}_e = \mathcal{R}_t \cdot S(t)$, where $\mathcal{R}_t$ reflects the current intervention regime. A low effective $\mathcal{R}_e$ is achieved either following an extensive exposure of the population to the virus (a low $S(t)$), or by imposing stringent restrictions to curb virus spread (low $\mathcal{R}_t$).

We can now formulate the outcomes of the optimal planning problem in these terms. The outcomes presented in the preceding section basically follow one of two basic paths.

Strong containment. This path implies that $\mathcal{R}_e$ is kept below or around 1 almost throughout the planning period with stringent restrictions (low $\mathcal{R}_t$), while preserving the pool of the susceptibles intact to a large extent (high $S(t)$). This path requires strong suppression measures to be imposed for long periods of time. These measures either reduce the epidemic or keep it growing at a very slow pace. The costs of loss of output are high, but the death toll is low.

Weak containment. This path implies that the reduction in $\mathcal{R}_e$ is obtained by the depletion of the susceptibles pool (a low $S(t)$), while policy interventions are loose or short-lived (resulting in a high $\mathcal{R}_t$). Since this path involves less prolonged and more delayed interventions, it is cheaper in terms of loss of output, while the ensuing death toll is inevitably high relative to the strong containment path.

These two policy paths reflect the fundamental trade-off between economic costs and death tolls in managing the epidemic. The resolution of the trade-off, the optimal policy choice, depends on a number of factors: the extent to which economic activity can be maintained in lockdowns, the fatality rate of the virus, and the value of statistical life. Even more critically, it depends on the type of policy instruments available to the planner. It turns out that when cyclical strategies are in the toolkit, the fundamental trade-offs can be softened in a way that allows achieving lower economic costs and/or lower death tolls, while waiting for vaccine arrival.

A key point about the cyclical strategies is that they average out k working days and $(14-k)$ lockdown days and therefore reduce $\mathcal{R}_t$. This approximation

[19] In this case

$$\begin{aligned} \mathcal{R}_e &= \mathcal{R}_t S^{HI}(t) = 1 \\ S^{HI}(t) &= \frac{1}{\mathcal{R}_t} \end{aligned}$$

[20] The demarcation value of 1.1 is arbitrary, but we find it to be useful for the current discussion.

of the average $\mathcal{R}_t$, to be denoted $\mathcal{R}_a$, is given by:[21]

$$\mathcal{R}_a(k) \simeq \frac{k \cdot \mathcal{R}_W + (14-k) \cdot \mathcal{R}_L}{14} < \mathcal{R}_W \tag{27}$$

From equation (27), it is immediately clear that the tighter, low-k strategies are more efficient in epidemic suppression as their reproduction number $\mathcal{R}_a$ is lower. Crucially, they can bring down the infection while not closing down the economy completely. These strategies can be applied over long time horizons and achieve the strong containment type of solution. The high-k strategies can only be compatible with strong containment when applied after a prolonged lockdown and for relatively short periods of time, not giving the epidemic enough time to vastly grow.

The optimal timings reported in Table 3 show how these different policy choices are implemented by the planner at the baseline parameter values. Table 4 elaborates on the associated $\mathcal{R}_a$ and $S(t)$ values.

Table 4: Dynamics Under the Cyclical Strategies – Baseline

Baseline: $\chi = 85, \rho = 0.65, IFR = 0.8\%$						
k	$k=3$	$k=4$	$k=5$	$k=6$	$k=7$	$k=8$
R_a	0.94	1	1.05	1.1	1.16	1.20
T_0	9	0	0	0	0	31
T_1	28	14	14	100	128	63
T_2	483	511	540	540	540	388
$S(T_0)$	1.00	1.00	1.00	1.00	1.00	0.96
$S(T_1)$	1.00	1.00	1.00	1.00	1.00	0.91
$S(T_2)$	0.99	1.00	0.98	0.98	0.93	0.72
$S(T_V)$	0.99	1.00	0.98	0.98	0.93	0.72
$R_e(T_0)$	0.8	0.8	0.8	0.8	0.8	0.77
$R_e(T_1)$	0.94	1	1.05	1.1	1.16	1.09
$R_e(T_2)$	1.49	1.5	1.47	1.47	1.40	1.08
D (per 10^6)	45	27	166	137	596	2,258
Containment	strong					weak

Notes:
$R_e(T_0) = S(T_0) \cdot R_L$ is the effective R at the beginning of lockdown.
$R_e(T_1) = S(T_1) \cdot R_a$ is the effective R at the beginning of the cyclical strategy
$R_e(T_2) = S(T_2) \cdot R_W$ is the effective R at the beginning of release.

[21] The average here is not exactly a linear function of $\mathcal{R}^W, \mathcal{R}^L$ and so this is an approximation.

The low-k strategies ($k = 3, 4, 5, 6, 7$) are used to achieve *strong containment*, where, by the time of vaccine arrival, no more than 7% of the population is exposed to the virus. As can be seen in Table 4, this is achieved by a very early lockdown phase followed by an extremely prolonged cyclical stage, which lasts up to vaccine arrival in most cases. Strong containment here is possible since the average reproduction $\mathcal{R}_a$ of these strategies is low, and so they achieve an effective $\mathcal{R}_e$ below or near unity, even though the pool of susceptibles remains largely intact. Within this group, the most stringent strategies ($k = 3, 4$) manage to bring down the disease. The less stringent strategies ($k = 5, 6, 7$) do not bring down the disease but do not allow it to grow fast before the vaccine arrives. They also require a longer initial lockdown. These dynamics can be seen in Figures 4 and 5 above.

The high-k strategy ($k = 8$) results in a *weak containment* solution. By the time the vaccine arrives, almost 30% of the population gets the virus; see the $S(T_V)$ value in Table 4. This is achieved by delaying the first lockdown by almost a month, and also by removing all interventions relatively early. The dynamics feature two waves: an initial eruption and its suppression with the first lockdown, and then another, smaller wave, during the cyclical strategy phase. This second wave is moderate because $\mathcal{R}_e$ in the latter stage is low despite a high $\mathcal{R}_a$, due to the depleted pool of susceptibles (see $S(T1)$ and $\mathcal{R}_e(T1)$ in Table 4). When the restrictions are lifted, the effective $\mathcal{R}_e$ is so low that there will be almost no disease growth. This, too, may be seen in Figures 4 and 5.

6.2 The Policy Frontier

As shown above, there are two major ways to deal with the epidemic: strong and weak containment. The timing of interventions, the ensuing epidemic dynamics, and realized costs all depend on the instruments available to the planner. The trade-offs involved are most easily seen in a two-dimensional graph, that maps the outcome obtained under each instrument on two axes – the death toll per million people and the value of lost output in annual GDP terms. One can trace out a policy frontier using this graphical representation. Panel a of Figure 6 presents this frontier. It does so for different values of k, ranging from 3 to 8, and for three different values of the value of life, χ (60, 85, 100).

Figure 6: The Policy Frontier

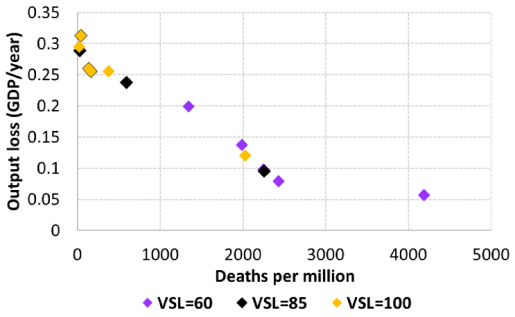

a. $\chi = 60, 85, 100$ and $k \in \{3, 4, 5, 6, 7, 8\}$

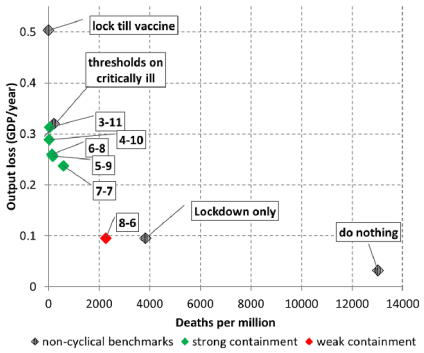

b. Baseline $\chi = 85$

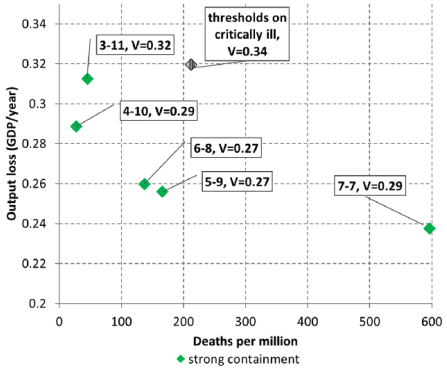

c. Baseline, zoomed in

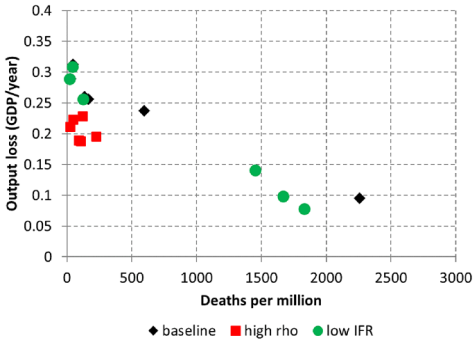

d. Parameter Variations

Panel a clearly shows that there exists a policy frontier. Note that for a large segment, the frontier is almost linear. In this part, deaths rise and output loss falls with an almost constant proportion, as the value of life, χ, falls. In the segments at the extremities it is almost vertical (on the left) and almost horizontal (on the right). This means that in those parts there is no tradeoff. When deaths are low, raising χ just increases output loss without much effect on deaths; when deaths are high, lowering χ just increases them more, without much gain in terms of output.

Panel b of the figure shows the frontier using just the baseline values, discussed in Section 4, i.e., with $\chi = 85$. It also shows the benchmark strategies, discussed in sub-section 3.6, marked by a mash. The two extreme benchmarks of locking the economy completely till vaccine arrival and not doing any intervention are represented by two extreme points on the graph, with huge output or death toll, respectively. The benchmark optimal lockdown policy ($k = 0$), denoted "lockdown only," lies above the frontier. Panel c magnifies part of this figure, showing that the thresholds strategy benchmark also lies above the frontier.

In panels b and c, the cyclical policy plans trace out the frontier, conditional on $\chi = 85$. The strategies marked in green follow strong containment policies. Hence they have a relatively high cost of lost output and a moderate death toll. These are low-k strategies with just a few days open each fortnight, and are located on the upper-left part of the graph. The cyclical strategy marked in red ($k = 8$) is not powerful enough to suppress the epidemic efficiently, as more open days are allowed every fortnight and therefore containment is weak. This strategy is located on the lower-right segment of the frontier, representing a high death toll with moderate output losses.

The figure clearly shows that the use of cyclical strategies brings about a very substantial improvement in outcomes relative to the two extremes of no intervention or full lockdown (as also seen in the values reported in Table 3). Compared to the optimal threshold strategy, the type of decision-making seen in reality, the cyclical strategies provide significant improvement too. Using Table 3 and Figure 6b, one can see that the $k = 8$ strategy provides some improvement in social welfare by lowering output loss. However this is done at the price of a higher death toll. It is the low-k cyclical strategies, especially $k = 5, 6$ that provide for a much more significant improvement. They lower output losses with small changes in the death toll, within a strong containment solution.

Panel a of Table 5 presents model outcomes with the alternative value of $\chi = 60$ as discussed above instead of the baseline case of $\chi = 85$.

Table 5
a. An Alternative Value of Life χ

value of life: $\chi = 60$						
k	$k=3$	$k=4$	$k=5$	$k=6$	$k=7$	$k=8$
T_0	36	32	0	33	31	31
T_1	56	56	14	56	49	52
T_2	99	371	540	360	325	332
$S(T_0)$	0.92	0.96	0.99	0.95	0.96	0.96
$S(T_1)$	0.84	0.91	0.99	0.89	0.93	0.92
$S(T_2)$	0.79	0.85	0.98	0.78	0.74	0.70
$S(T_V)$	0.55	0.84	0.98	0.77	0.72	0.70
V	0.31	0.28	0.27	0.26	0.23	0.22
V_Y	0.06	0.20	0.26	0.14	0.10	0.08
V_D	0.25	0.08	0.01	0.12	0.13	0.14
D (per 10^6)	4,194	1,348	166	1,987	2,250	2,432
Containment	weak		strong	weak		

b. Parameter Variations - ρ and IFR

V		
	$\rho = 0.75$	$IFR = 0.6\%$
Cyclical:		
$k=3$	0.23	0.31
$k=4$	0.21	0.29
$k=5$	0.20	0.27
$k=6$	0.20	0.26
$k=7$	0.21	0.24
$k=8$	0.24	0.23
Non-cyclical:		
$k=0$	0.31	0.36
Thresholds	0.24	0.32

Notes: See Table 3.

Table 5a shows in numbers what is seen in panel a of Figure 6 graphically: though the location of the frontier does not visibly change as χ declines, the points move to the lower-right corner, i.e., to the region of weak containment. Even when armed with the most stringent instruments ($k = 3$ and $k = 4$), previously used to keep the disease under strict control, the planner now chooses weak containment. This is so because the economic costs of these very restrictive strategies do not justify using them for prolonged suppression when life is less valuable. Only the $k = 5$ cyclical strategy that is characterized by both suppression efficiency and moderate output costs is still used to implement the strong containment solution.

The trade-offs embodied in the frontier graph and the planner optimal choices depend on the lockdown severity parameter ρ (the fraction of working in lockdown) and on the infection fatality rate. We explore the sensitivity of outcomes to these parameters next.

6.3 Parameter Variations

Panel d in Figure 6 and panel b in Table 5 present the results with a higher $\rho = 0.75$, i.e., employment is at 75% of its steady state level during lockdown, and, separately, with an alternative IFR value of 0.6%.

Higher ρ means output losses from lockdowns are less severe; thus the planner can aim for strong containment, which is now less costly. Hence the policy frontier is to the left of the baseline frontier, and concentrated on the left hand side of the graph. Even the weakest (high-k) instrument is now used for strong containment, which is achieved by applying a very prolonged initial lockdown followed by a short cyclical phase.

A lower fatality rate moves the frontier leftwards, to lower death tolls. This shift is more pronounced at the lower-right end of the frontier, where weak containment solutions are located. These solutions rely on high exposure of the population to the disease. When the death probability declines, fatalities drop significantly, and so the frontier moves perceptibly. Such solutions are now optimal under a wider range of instruments. Facing a lower fatality rate, the planner is more inclined to open more and thus reduce output costs, in exchange for somewhat higher death tolls. In the strong containment solutions located at the upper-left region of the frontier, exposure to the disease is low to begin with. Even though the fatalities rate goes down, the decline in the death toll is small in absolute terms.

As seen in panel b of Table 5, the advantage of the cyclical tools relative to the benchmarks is preserved under these parameter variations.

7 The Cyclical Strategies vs Actual Experience

The cyclical strategies can be compared to actual real world experience. We do so by simulating optimal plans under the cyclical strategies and comparing them to a policy path based on the experience of the states of New York

and Florida. The choice of these two states is motivated by the fact that both experienced high levels of the epidemic but very different dynamics.

7.1 Data and Methodology

We use daily death data.[22] In both New York State and Florida, it spans 275 days, from March to November 2020. This is the sum of confirmed and probable deaths from COVID19. The death count is smoothed using a 7-day centered moving average.

The methodology we use is as follows.

(i) Estimation of disease growth rates to obtain initial guesses of the reproduction number at various stages of the epidemic.[23]

(ii) Estimation of the reproduction number at various stages of the epidemic by minimizing squared deviations of the simulated series of daily deaths and the corresponding data series, using the estimated rates in (i) as starting values.

(iii) Using the derived parameter values for simulation of the optimal cyclical strategies and for simulation of the policy path based on actual experience.

In what follows we elaborate on these steps.

(i) Estimation of disease growth rates

We use the following relations. At the start of the epidemic $S(t) \simeq 1$. The path of $I(t) = I_1(t) + I_2(t)$ is postulated to be:

$$I(t) = I(0)\, e^{\lambda t} \tag{28}$$

For the model in use, i.e., a $SEIR$ model with 2 sub-compartments, λ satisfies the following relation (using equation 4 in Wearing et al (2005)):

$$\mathcal{R} = \frac{\lambda\left(\frac{\lambda}{2\sigma}+1\right)^2}{\gamma\left(1-\left(\frac{\lambda}{2\gamma}+1\right)^{-2}\right)} \tag{29}$$

At later stages, as the amount of susceptibles declines, the effective reproduction number $\mathcal{R}_e$ is given by

$$\mathcal{R}_e = S(t) \cdot \mathcal{R}_t \tag{30}$$

We estimate λ, the growth rate of $I(t)$, the infected, employing daily death data. Using the values of γ and σ from Table 2, we derive the value of $\mathcal{R}_0$ from equation (29) for the initial outbreak period. We subsequently use equations (29) and (30) to derive $\mathcal{R}_L$ for the lockdown period.

To estimate λ we run a Poisson (log-linear) regression as follows:

$$\log\left(\textit{daily death count}\right) = \textit{const} + \lambda t \tag{31}$$

[22] The data are taken from COVID-19 Data Repository by the Center for Systems Science and Engineering (CSSE) at Johns Hopkins University, https://github.com/CSSEGISandData/COVID-19

[23] Throughout, the underlying assumption is that there is a constant generation interval (see sub-section 3.1).

(ii) Derivation of parameter values.

In the case of NYS, which experienced one wave of the epidemic between March and November 2020, to derive parameter values needed for the simulations, we solve the following minimization problem:

$$\min_{T_0,T_1,\mathcal{R}_0,\mathcal{R}_W,\mathcal{R}_L,\tau_0} \int_{t=0}^{t_{end}} \left(D\left(t\right) - D_{actual}\left(t-\tau_0\right)\right)^2 dt \tag{32}$$

where D_{actual} is the data death series and $D(t)$ is the data death series solved from our $SEIR$ model; τ_0 is the time needed to adjust the death series to model dynamics, given the duration from infection to death; lockdown is imposed between T_0 and T_1 so thus

$$\mathcal{R} = \begin{cases} \mathcal{R}_0 & t \leq T_0 \\ \mathcal{R}_L & T_0 < t \leq T_1 \\ \mathcal{R}_W & T_1 < t \end{cases}$$

We solve the minimization problem by an exhaustive grid search, where τ_0, T_0, T_1 are positive integers, $T_1 > T_0$, and $\mathcal{R}_0, \mathcal{R}_L, \mathcal{R}_W$ are on a grid with 0.1 precision around the initial values. We use the calibrated values presented in Table 2 above.[24] Initial values are derived in step (i) above. We thus derive the control variables of problem (32), namely $T_0, T_1, \mathcal{R}_0, \mathcal{R}_W, \mathcal{R}_L, \tau_0$.

In the case of Florida, which has experienced two epidemic waves, we are solving an expanded problem in a similar way. The minimization problem is given by:

$$\min_{\widetilde{X}_0,\widetilde{X}_R,\widetilde{X}_L,\mathcal{R}_0,\mathcal{R}_W,\mathcal{R}_L,\tau_0} \int_{t=0}^{t_{end}} \left(D\left(t\right) - D_{actual}\left(t-\tau_0\right)\right)^2 dt \tag{33}$$

where lockdown is imposed when $X > \widetilde{X}_0$, released when $X < \widetilde{X}_R$, and re-imposed when $X > \widetilde{X}_L$. Now:

$$\mathcal{R} = \begin{cases} \mathcal{R}_0 & \text{initially} \\ \mathcal{R}_L & X > \widetilde{X}_0 \text{ for the first time} \\ \mathcal{R}_W & X < \widetilde{X}_R \text{ (first lockdown is at least 14 days)} \\ \mathcal{R}_L & X > \widetilde{X}_L \end{cases}$$

We derive the control variables of problem (33), namely $\widetilde{X}_0, \widetilde{X}_R, \widetilde{X}_L, \mathcal{R}_0, \mathcal{R}_W, \mathcal{R}_L, \tau_0$.

(iii) Using the derived parameter values.

Using the derived values of $\mathcal{R}_0, \mathcal{R}_W, \mathcal{R}_L$ we simulate the optimal cyclical strategies and actual experience.

7.2 Results

We first report the results with respect to growth dynamics and the reproduction parameter. We subsequently present the outcomes of the simulated optimal strategies and compare them to actual experience.

[24] We use the same IFR as in Table 2, based on the findings of IHME COVID-19 Forecasting Team (2021).

7.2.1 Growth Dynamics and the Reproduction Parameter

In NYS the exponential growth rate λ is estimated using equation (31) between March 11 and March 30, 2020 to be 0.23 with a 95% confidence interval of $[0.22, 0.25]$. In the model, these values correspond to $\mathcal{R}_0 = 3.17$ $[2.95, 3.42]$. The exponential decline rate λ is estimated between April 8 and July 28, 2020 to be -0.0456 with a 95% confidence interval of $[-0.0464, -0.0447]$.

Our procedure, which was elaborated in sub-section 7.1, yields the result that 12 days after the beginning of lockdown, on March 30, 2020, 11% of the population were already infected, so $S = 0.89$. This is consistent with the serological findings of Richardson et al (2020). Thus $\mathcal{R}_L = \mathcal{R}_e/0.89$. Under $SEIR$, these λ values correspond to $\mathcal{R}_L = 0.84$ $[0.83, 0.85]$.

We further estimate the exponential growth rate following the release from lockdown, λ_W, as 0.018 $[0.016, 0.02]$. At release, we find that 18% of the population had been infected (broadly consistently with the afore-cited reference) so $S = 0.82$ and $\mathcal{R}_W = 1.36$ $[1.34, 1.37]$. This value of $\mathcal{R}_W$ generates an effective $\mathcal{R}_e = 0.82 * \mathcal{R}_W = 1.15$ leading to a slow increase of the daily death series, as seen in the data.

In Florida the exponential growth rate λ is estimated using equation (31) between March 17 and April 1, 2020 to be 0.21 with a 95% confidence interval of $[0.19, 0.23]$. In the model, these values correspond to $\mathcal{R}_0 = 2.89$ $[2.65, 3.13]$. The exponential decline rate λ is estimated between May 5 and May 28, 2020 to be -0.02 with a 95% confidence interval of $[-0.023, -0.016]$.

Our procedure yields the result that only 1.3% of the population were infected, so $S = 0.987$. Thus $\mathcal{R}_L = \mathcal{R}_e/0.987$. In the model, these λ values correspond to $\mathcal{R}_L = 0.89$ $[0.88, 0.91]$.

We further estimate the exponential growth rate following release from lockdown, λ_W, as 0.043 $[0.041, 0.045]$.During the period of release following the first wave in Florida, we find that 3% of the population had been infected so $S = 0.97$ and $\mathcal{R}_W = 1.32$ $[1.30, 1.34]$.

7.2.2 Simulated Policy Strategies

We simulate a model of lockdown policy so as to generate a death series comparable to actual data. This will enable us to see how close the model is to the data. As initial values we use the ones obtained in step (i) of the procedure elaborated in sub-section 7.1. In NYS, the solution yields the following values: $\mathcal{R}_0 = 3.21$, $\mathcal{R}_L = 0.86$, $\mathcal{R}_W = 1.36$. In Florida, the solution yields the following values: $\mathcal{R}_0 = 3.12$, $\mathcal{R}_L = 0.92$, $\mathcal{R}_W = 1.34$. These values, which are very close to the initial ones, minimize the distance between the actual and simulated death series. How good is the data fit? Table 6 reports moments of the data series and the simulated one.

Table 6
Moments of the Cumulative Deaths Series, Simulation and Data

a. NYS

	simulation	**data**	**p value of equality test**
mean	0.0014	0.0014	0.62
median	0.0017	0.0017	0.72
std	0.0006	0.0006	0.79
skewness	−1.73	−1.65	
kurtosis	4.43	4.13	
correlation	0.9986		

b.Florida

	simulation	**data**	**p value of equality test**
mean	0.0003	0.0003	0.93
median	0.0002	0.0002	0.72
std	0.0003	0.0003	0.79
skewness	0.25	0.41	
kurtosis	1.37	1.60	
correlation	0.9937		

Notes:
1. The computations are explained in sub-section 7.1.
2. Test of moment equality are t-test for mean, Wilcoxon/Mann-Whitney test for median, and F-test for variance. A high p value means that the null of moments equality cannot be rejected.

Source:
The data are taken from the COVID-19 Data Repository, the Center for Systems Science and Engineering (CSSE) at Johns Hopkins University,
https://github.com/CSSEGISandData/COVID-19.

By all moments, the simulated and actual series for cumulative deaths (smoothed) are very close, suggesting a very good fit. This point is important as it shows that the model is able to reproduce the data.

Next, we simulate the optimal cyclical strategies using the same reproduction parameter values. Figure 7 shows the outcome using the frontier, in terms similar to Figure 6; panel a presents NYS and panel b presents Florida. Note that the optimization was done for the entire two year horizon, as above, but Figure 7 presents the cumulative results only for the period from March 1 to November 30, 2020. As actual state-level employment data from BLS (CES) are in monthly terms, we adapt the computation to discrete time, monthly terms. Details are provided in online Appendix B.

Figure 7: Cyclical Strategies vs Actual Experience, March to November 2020

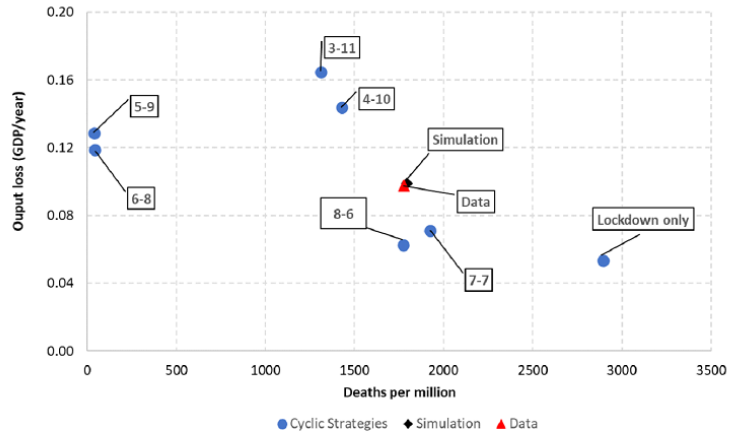

a. New York State

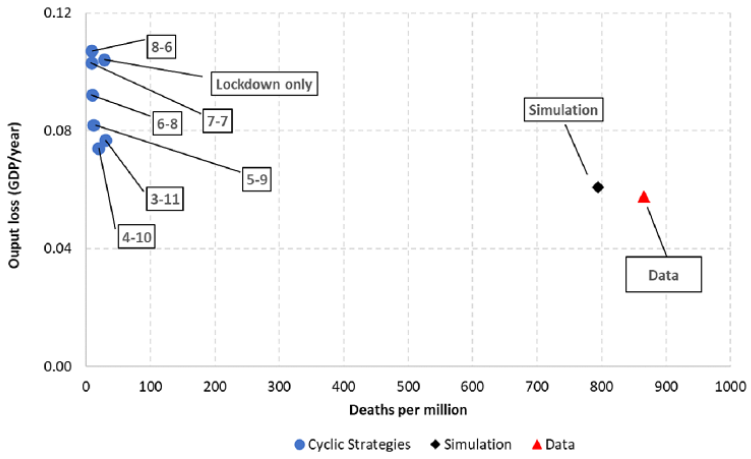

b. Florida

The figure shows the outcomes of the cyclical strategies, with k ranging from 0 (optimal lockdown) to 8, the simulated actual experience, and the data. The last two points are very close as the fit is good. Table 7 presents the values shown on the figures axes as well as total planner cost, V. Note that in each panel of the table we present the parameter values relevant for the state in question.[25]

Table 7
a. New York State, March 1 – November 30

$\rho = 0.65, IFR = 0.8\%, \chi = 85, \overline{X} = 0.00023$			
	deaths per million	Output loss Vy	V
lockdown only	2,895	0.05	0.30
$k = 3$	1,312	0.16	0.28
$k = 4$	1,428	0.14	0.26
$k = 5$	38	0.13	0.13
$k = 6$	42	0.12	0.12
$k = 7$	1,922	0.07	0.23
$k = 8$	1,774	0.06	0.21
Actual experience simulation	1,792	0.10	0.25
Data	1,779	0.10	0.25

b. Florida, March 1 – November 30

$\rho = 0.85, IFR = 0.8\%, \chi = 85, \overline{X} = 0.00028$			
	deaths per million	Output loss Vy	V
lockdown only	28	0.10	0.11
$k = 3$	30	0.08	0.08
$k = 4$	19	0.07	0.08
$k = 5$	12	0.08	0.08
$k = 6$	9	0.09	0.09
$k = 7$	9	0.10	0.10
$k = 8$	9	0.11	0.11
Actual experience simulation	795	0.06	0.13
Data	866	0.06	0.13

[25]The fraction of workers in employment in lockdowns in New York State is calibrated to our baseline US value ($\rho = 0.65$). For Florida, the BLS (CES) employment statistics indicate that during the period of the 'stay-at-home' order (in the month of April 2020), the share was relatively high, at 87%. Additionally, we numerically search for the ρ value that would generate the same employment losses in our fatalities-fitting exercise as in the data, and the resulting ρ is 0.85. Therefore, we adopt a value $\rho = 0.85$ for Florida. As the source data for $\overline{X}$ we continue to use Harvard Global Health Institute at https://globalepidemics.org/our-data/hospital-capacity/.

Notes:
The computations are explained in sub-section 7.1.

7.3 Discussion

Figure 7 and Table 7 show that the cyclical strategies perform better than actual experience. The data points lie above the (imaginary, unplotted) frontier. Total planner discounted cost, in annual GDP terms, goes down from 25% to 12% in NYS and from 13% to 8% in Florida. Why so?

In New York, the low k cyclical strategies achieve strong containment, resulting in a much lower death rate, and in only a small increase in output loss. In fact even the high k strategies, which achieve only weak containment, are better than the actual outcomes. Their death rates are lower or only slightly higher and output loss is significantly lower. It is clear that actual policy underperformed, and achieved only weak containment. In particular, the use of moderately stringent $k = 5$ and $k = 6$ cyclical tools implies a dramatic reduction in the death toll and only a slight increase in output costs relative to actual experience. Timing is key here – the optimal use of $k = 5$ and $k = 6$ involves an immediate initial lockdown, which proves to be critical in curbing the disease during its exponential growth phase. Compared to this optimal policy, in the simulated actual experience, waiting with initial lockdown, resulted in death tolls that are higher by a factor of 45.[26] It appears that lockdown in New York State was relatively late and thus a significant outbreak was facilitated.

In Florida, all cyclical strategies achieve strong containment while the actual outcome, similar to New York State, is one of weak containment. The gain, relative to actual experience, is similar to the low k case in New York, namely low death rates with only a slight increase in output loss. With a high fraction of economic activity maintained during lockdown in Florida, the model implies that stringent lockdowns should have lasted much longer, suppressing the disease without dramatic damage to output. The intuition for this result is that actual release from lockdown in Florida in practice was relatively fast and so renewed progression of the epidemic was facilitated.[27]

Note, too, that the superior outcomes of the cyclical policies are achieved despite the fact that we constrain the planner in the cases of those policies to choose only three points in time, while in the real world cases there were fewer constraints.

8 Conclusions

Given the significant trade-offs between health outcomes (deaths, breaches of ICU capacity) and economic outcomes (loss of output and employment), the analysis has shown that pandemic management policy based on time restrictions may lead to significant improvement. The improvement was quantified in

[26] The importance of early NPIs for curbing cumulative death tolls has been stressed in the epidemiological literature on the 1918 Influenza Pandemic (see, for example, Markel, Lipman, Navarro, Sloan, Michalsen, Stern, and Cetron (2007) and Bootsma and Ferguson (2007)). Hatchett, Mecher, and Lipsitch (2007) highlight the fact that the effects of early NPIs may be especially pronounced over short horizons, but are still significant in terms of overall cumulative mortality.

[27] This can be seen in panel a of Figure 1.

terms of social welfare, evaluated in PDV, annual GDP terms. The comparison was made relative to four hypothetical benchmarks, as well as to the experience of New York State and Florida. The analysis, which is relevant for COVID 19 as well as for any future epidemic, laid down the principles for time restrictions policy, as well as a framework for comparative policy analysis.

Exploring this policy seems a promising avenue for future research in the context of managing epidemics. The analysis clearly shows that such strategies allow for a nuanced response to observed epidemic dynamics, without resorting to single out any population group. It is important to note that the afore-mentioned advantages of the cyclical strategies over prevalent policies are likely to be a lower bound of their full benefits. First, in our model the planner is deliberately constrained in the way cyclical tools are applied; for example, not permitted to mix within the set of strategies, or apply them in a staggered way. Giving the planner additional degrees of freedom, as we do for the benchmark thresholds strategies, should increase the advantages of the novel instruments over prevalent policies. Second, and not less significant, our model does not allow us to quantify the additional benefits of cyclical tools, such as the predictability of production that they entail, as well as their potential to alleviate part of the negative impact of prolonged isolation on mental well-being.

References

[1] Abel, Andrew B. and Stavros Panageas, 2020. "Optimal Management of a Pandemic in the Short Run and the Long Run," NBER Working Paper No. 27742.

[2] Abell, Martha L. and James P. Braselton, 2016. **Differential Equations with Mathematica**, 4th edition, Academic Press.

[3] Acemoglu, Daron, Victor Chernozhukov, Ivan Werning, and Michael D. Whinston, 2020. "A Multi-Risk SIR Model with Optimally Targeted Lockdown" **AER Insights**, forthcoming.

[4] Alon, Uri, Ron Milo, and Eran Yashiv, 2020. "10-4: How to Reopen the Economy by Exploiting the Coronavirus's Weak Spot," **The New York Times,** May 11**.**

[5] Alon, Uri and Eran Yashiv, 2020. "Exploiting a coronavirus weak-spot for an exit strategy," **VoxEU.org,** 27 April.

[6] Alvarez, Fernando, David Argente, Francesco Lippi, 2020. "A Simple Planning Problem for COVID-19 Lockdown,"**AER Insights**, forthcoming.

[7] Atkeson, Andrew G., Karen Kopecky, and Tao Zha, 2021. "Behavior and the Transmission of COVID-19," **AER Papers and Proceedings,** forthcoming.

[8] Avery, Christopher, William Bossert, Adam Clark, Glenn Ellison, and Sara Fisher Ellison, 2020. "An Economist's Guide to Epidemiology Models of Infectious Disease" **Journal of Economic Perspectives** 34, 4, 79–104

[9] Baqaee, David, Emmanuel Farhi, Michael Mina, and James H. Stock, 2020. "Policies for a Second Wave," **Brookings Papers on Economic Activity**, **Special edition 2020: COVID-19 and the economy.**

[10] Bar-On, Yinon, Tanya Baron, Ofer Cornfeld, Ron Milo and Eran Yashiv, 2021. "COVID19: Erroneous Modelling and Its Policy Implications," working paper.

[11] Bar-On, Yinon, Ron Sender, Avi Flamholz, Rob Phillips, and Ron Milo, 2020. "A Quantitative Compendium of COVID-19 Epidemiology," arXiv:2006.01283; available at https://arxiv.org/abs/2006.01283

[12] Bloom, David E., Michael Kuhn, and Klaus Prettner, 2020. "Modern Infectious Diseases: Macroeconomic Impacts and Policy Responses," NBER Working Paper No. 27757.

[13] Bootsma, Martin CJ, and Neil M. Ferguson, 2007. "The Effect of Public Health Measures on the 1918 Influenza Pandemic in US Cities." **Proceedings of the National Academy of Sciences** 104, 18, 7588-7593.

[14] Champredon, David, Jonathan Dushoff, and David J.D. Earn, 2018. "Equivalence of the Erlang-distributed SEIR Epidemic Model and the Renewal Equation," **SIAM Joural of Applied Math** 78, 6, 3258–3278.

[15] Dingel, Jonathan I. and Brent Neiman, 2020. "How Many Jobs Can be Done at Home?" **Journal of Public Economics** 189, 104235.

[16] Eichenbaum, Martin S., Sergio Rebelo, and Mathias Trabandt, 2020. "The Macroeconomics of Epidemics," NBER Working Paper No. 26882.

[17] Farboodi, Maryam, Gregor Jarosch, and Robert Shimer, 2020. "Internal and External Effects of Social Distancing in a Pandemic," NBER Working Paper No. 27059.

[18] Fernandez-Villaverde, Jesus and Chales I. Jones, 2020. "Estimating and Simulating a SIRD Model of COVID-19 for Many Countries, States, and Cities," NBER Working Paper No. 27128.

[19] Garibaldi, Pietro, Espen R. Moen, and Christopher A. Pissarides, 2020. "Modelling Contacts and Transitions in the SIR Epidemics Model," **Covid Economics** 5, 16 April.

[20] Greenstone, Michael and Vishan Nigam, 2020. "Does Social Distancing Matter?" BFI working paper no. 2020-26

[21] Hale, Thomas , Sam Webster, Anna Petherick, Toby Phillips, and Beatriz Kira, 2020. **Oxford COVID-19 Government Response Tracker.** Blavatnik School of Government.

[22] Hall, Robert E, Charles I. Jones, and Peter J. Klenow, 2020. "Trading Off Consumption and COVID-19 Deaths," **Minneapolis Fed Quarterly Review** 42, 1, 2-14.

[23] Hamermesh, Daniel S., 2020. "Lockdowns, Loneliness and Life Satisfaction," IZA Discussion Paper No. 13140.

[24] Hatchett, Richard J., Carter E. Mecher, and Marc Lipsitch, 2007. "Public Health Interventions and Epidemic Intensity During the 1918 Influenza Pandemic." **Proceedings of the National Academy of Sciences** 104, 18, 7582-7587.

[25] He, X., E.H.Y. Lau, P. Wu, et al., 2020. "Temporal Dynamics in Viral Shedding and Transmissibility of COVID-19." **Nature Medicine** 26, 672–675. https://doi.org/10.1038/s41591-020-0869-5

[26] Huang, Chaolin, Yeming Wang, Xingwang Li, Lili Ren, Jianping Zhao, Yi Hu, et al., 2020. "Clinical Features of Patients Infected with 2019 Novel Coronavirus in Wuhan, China," **Lancet** 395: 497–506. https://doi.org/10.1016/S0140-6736(20)30183-5

[27] IHME COVID-19 Forecasting Team, Reiner, R.C., Barber, R.M. et al., 2021. "Modeling COVID-19 Scenarios for the United States." **Nature Medicine** 27, 94–105. https://doi.org/10.1038/s41591-020-1132-9

[28] Imperial College COVID-19 Response Team, 2020. "Report 13: Estimating the number of infections and the impact of non-pharmaceutical interventions on COVID-19 in 11 European countries," https://dsprdpub.cc.ic.ac.uk:8443/bitstream/10044/1/77731/10/2020-03-30-COVID19-Report-13.pdf

[29] International Monetary Fund, 2020. **World Economic Outlook: A Long and Difficult Ascent**. Washington, DC, October.

[30] Johns Hopkins University CSSE, 2020. "2019 Novel Coronavirus COVID-19 (2019-nCoV) Data Repository," Center for Systems Science and Engineering.

[31] Jones, Callum J., Thomas Philippon, and Venky Venkateswaran, 2020. "Optimal Mitigation Policies in a Pandemic: Social Distancing and Working from Home," NBER Working Paper No. 26984.

[32] Kaplan, Greg, Ben Moll, and Gianluca Violante, 2020. "The Great Lockdown and the Big Stimulus: Tracing the Pandemic Possibility Frontier for the U.S." NBER Working Paper No. 27794

[33] Karin, Omer, Yinon Bar-On, Tomer Milo, Itay Katzir, Avi Mayo, Yael Korem, Avichai Tendler, Boaz Dudovich, Eran Yashiv, Amos J Zehavi, Nadav Davidovitch, Ron Milo and Uri Alon,

2020. "Adaptive Cyclic Exit Strategies from Lockdown to Suppress COVID-19 and Allow Economic Activity", MedRxiv, https://www.medrxiv.org/content/10.1101/2020.04.04.20053579v4.full.pdf

[34] Kermack, William O., and Anderson G. McKendrick, 1927. "A Contribution to the Mathematical Theory of Epidemics," **Proceedings of the Royal Society London**. Ser. A., 115, 700–721.

[35] Kotz, Samuel and Saralees Nadarajah, 2000. **Extreme Value Distributions: Theory and Applications**. World Scientific, Singapore.

[36] Krueger, Dirk, Harald Uhlig, and Taojun Xie, 2020. "Macroeconomic Dynamics and Reallocation in an Epidemic," NBER Working Paper No. 27047

[37] Li, Ruiyun , Sen Pei, Bin Chen, Yimeng Song, Tao Zhang, Wan Yang, and Jeffrey Shaman, 2020. "Substantial Undocumented Infection Facilitates the Rapid Dissemination of Novel Coronavirus (SARS-CoV-2)," **Science** 368(6490), 489-493.

[38] Markel, Howard, Harvey B. Lipman, J. Alexander Navarro, et al., 2007. 'Nonpharmaceutical Interventions Implemented by US Cities During the 1918-1919 Influenza Pandemic" **JAMA** 298, 6, 644-654.https://doi:10.1001/jama.298.6.644

[39] Mills, Christina E., James M. Robins, and Marc Lipsitch, 2004. "Transmissibility of 1918 Pandemic Influenza, " **Nature** 432, 904-906.

[40] Richardson Safiya, Jamie S. Hirsch, Mangala Narasimhan, et al., 2020. "Presenting Characteristics, Comorbidities, and Outcomes Among 5700 Patients Hospitalized With COVID-19 in the New York City Area." **JAMA** 323(20):2052–2059.

[41] Salje, Henrik, Cecile Tran Kiem, Noemie Lefrancq, Noemie Courtejoie, Paolo Bosetti, Juliette Paireau, et al., 2020. "Estimating the Burden of SARS-CoV-2 in France," **Science** 369, 208–211. https://doi.org/10.1126/science.abc3517

[42] Tian, Huaiyu Yonghong Liu, Yidan Li, Chieh-Hsi Wu, Bin Chen, Moritz U. G. Kraemer, Bingying Li, et al., 2020. "An Investigation of Transmission Control Measures During the First 50 Days of the COVID-19 Epidemic in China," **Science** 368(6491), 638-642. https://doi.org/10.1126/science.abb6105

[43] Wallinga,Jacco, Michiel van Boven, and Marc Lipsitch, 2010. " Optimizing Infectious Disease Interventions During an Emerging Epidemic" **Proceedings of the National Academy of Sciences** 107, 2, 923–928.

[44] Wearing, Helen J., Pejman Rohani, and Matt J. Keeling, 2005. " Appropriate Models for the Management of Infectious Diseases," **PLoS Medicine** 2, 7, 621-627.

[45] Yashiv, Eran, 2020. "How to Reopen Society More Quickly," **Financial Times,** April 21.

March 16, 2021

Online Appendices When to Lock, Not Whom: Managing Epidemics Using Time-Based Restrictions

by Bar-On, Baron, Cornfeld, Milo, and Yashiv

Appendix A: Rationale, Implementation, and Advantages of the Cyclical Strategies

We spell out the proposed policy based on time restrictions, employing a cyclical schedule. This policy is extensively analyzed from an epidemiological perspective in Karin et al. (2020).

Background. As shown in Section 2, COVID 19 lockdowns are widely used, with substantial economic costs. Additionally and importantly, there are big costs related to well-being (see, for example, Hamermesh (2020)) that cannot be expected to be borne indefinitely. At the same time, second and third waves have materialized in many places. The strategy in question is meant to bridge between lockdown and release in a way which lessens the trade-off between managing the epidemic and sustaining the economy. In the main text we offer an extensive analysis of this point.

The basic idea. Following an initial lockdown, move to a regime of k days of work and $14-k$ days of lockdown, every 14 days. On work days, people are released from lockdown with strict hygiene and physical distancing measures on the same k weekdays for everyone. On lockdown days, people are kept away from work places as well as from other public spaces. Epidemiological measures need to be used throughout, including rapid testing, contact isolation, and compartmentalization of workplaces.

The rationale for this policy is as follows. Cyclical strategies reduce the average value of the reproduction parameter – which will be shown below to capture the progress of the disease – through two effects: time-restrictions and anti-phasing.

The time-restrictions effect is a reduction in the time T that an infectious person is in contact with many others, compared to the situation with no lockdown. For example, a 4-day work, 10-day lockdown cycle ($k = 4$) reduces T to $\frac{4}{14}T \approx 0.3T$. The anti-phasing effect uses the timescales of the virus against itself. Most infected people are close to peak infectiousness for about 3-5 days, beginning after a latent period of about 3 days (on average) after exposure. A proper work-lockdown cycle, such as a 4-work 10-lockdown schedule, allows most of those infected during work days to reach maximal infectiousness during lockdown, thus avoid infecting many others. Those with significant symptoms can be infectious for longer, but remain hospitalized, isolated, or quarantined along with their household members, preventing secondary infections outside the household.

Countries, regions or organizations that adopt this strategy are predicted to resist infections from the outside. An infection entering from the outside cannot spread widely because average $\mathcal{R}$ is below 1; we elaborate on this issue in subsection 6.1 in the main text. Intuitively, this result is due to the fact that, when taking into account the overall effects of $\mathcal{R}$ under work conditions and under lockdown conditions, the proposed cyclical strategy brings the average effective $\mathcal{R}$ to below 1. Hence, an infectious person entering from the outside and adhering to the cyclical strategy will on average infect less than one additional person in the region/organization. This implies that, with time, infections originating from infectious people entering from the outside will decay and not spark new outbreaks.

Context. Measures are required during work days to ensure that people do not excessively compensate for the lockdown periods by having so many more social connections so that infection is significantly increased. This includes sound epidemiological measures such as the continuation of banning large social gatherings, which bear the risk of superspreader events, and clear communication campaigns by health authorities to enhance adherence to hygiene and physical distancing.

Applicability. The proposed strategy can be applied at many levels – national, regional, metropolitan, institution, or firm; see the discussion in Online Appendix A. It may well be relevant, with the appropriate modifications, for other pandemics and epidemics. The world has already encountered quite a number of those over the past 40 years. Indeed. the set of epidemics since 1980 is quite large and includes, inter alia, HIV/AIDS, SARS, H5N1, Ebola, H7N9, H1N1, Dengue fever, and Zika (see Bloom, Kuhn, and Prettner (2020)).

Implementation. The cyclical strategy can be applied on many scales: firms, schools, towns, regions, or an entire country. In practice it has been implemented, or is under consideration, by:

(i) Multinational firms, including MasterCard, Delvenia, SENER, and Biogen

(ii) Schooling institutions – the Austrian school system, schools in and around Atlanta (GA), a local school district in Berkeley (CA), schools in Los Angeles (CA) and Minneapolis (MN).

(iii) Academic institutions – departments at Yale University, Cornell University, University of Georgia, and the University of Wisconsin-Madison.

(iv) Local government – Mexico City, NYC Department of Citywide Administrative services, and the City of Tubaro, Brazil.

The web site https://cyclicexitstrategy.org/ provides updated information.

Advantages. This paper thoroughly investigates the social welfare gains in terms of death tolls and economic losses. We elaborate in Sections 6 and 7 of the main text. Beyond that, the following advantages of these strategies can be noted.

(i) The cyclical strategy is not predicated on massive testing and can work in regions with insufficient testing capacity.

(ii) In countries or states with a large informal sector, adhering to continuous lockdown may be untenable, so the cyclical strategies are a solution.

(iii) The cyclical strategy provides economic opportunity during work days that may presumably improve adherence during lockdown days.

(iv) Implementation in schools is particularly important, serving to avoid significant educational costs.

(v) The cyclical strategy provides predictability and allows for rational planning of consumption and production decisions.

(vi) The policy is easy to communicate and transparent.

(vii) The policy is fair, not treating sectors or population groups differentially.

Appendix B: Computation of Planner Costs

The expression for planner cost over months 1 to M in discrete time, the analog of the continuous time formulation in the paper, is given by:

$$V = \sum_{t=1}^{M} \frac{1}{(1+r_m)^t} \left(\frac{Y^{SS,\cdot monthly}}{N^{SS}} \left(N^{SS} - N(t) \right) + \chi \cdot Y^{SS} \cdot \Delta D(t) \right)$$

where $Y^{SS,\cdot monthly}$ is the steady-state output in a month:

$$Y^{SS,\cdot monthly} = \frac{1}{12} Y^{SS}$$

Therefore:

$$V = \sum_{t=1}^{M} \frac{1}{(1+r_m)^t} \left(\frac{1}{12} Y^{SS} \left(1 - \frac{N(t)}{N^{SS}} \right) + \chi \cdot Y^{SS} \cdot \Delta D(t) \right)$$

The cost in units of annual output is:

$$\frac{V}{Y^{SS}} = \underbrace{\frac{1}{12} \sum_{t=1}^{M} \frac{1}{(1+r_m)^t} \left(1 - \frac{N(t)}{N^{SS}} \right)}_{V_Y\_discrete} + \underbrace{\chi \cdot \sum_{t=1}^{M} \frac{1}{(1+r_m)^t} \Delta D(t)}_{V_D\_discrete}$$

where $V_Y\_discrete$ is the discrete-time equivalent of the V_Y, computed over M months.

We compute $V_Y\_discrete$ in the data; we get $N(t)$ in each month from BLS CES employment data, and we construct N^{SS} in each month by projecting the January 2020 employment forward using monthly employment growth rates from 2018-2019. We compute $V_Y\_discrete$ in the simulation because it produces the series of $\frac{N(t)}{N^{SS}}$ in each day and we take the monthly average of the series.

We compute $V_D\_discrete$ for each month in the data based on the state-level daily death series from COVID-19 Data Repository by the Center for Systems Science and Engineering (CSSE) at Johns Hopkins University, in conjunction with the latest estimates of state population from US Census. We compute $V_D\_discrete$ in the simulation aggregating the daily deaths fraction over months. This way we can compute V/Y^{SS} both in the data and in the model for our state-level exercises in exactly the same terms as in our theoretical sections.

Appendix C: Recovering $\mathcal{R}_t$ from Daily Deaths Data, Adaptation to the SEIR Model

We apply the Fernandez-Villaverde and Jones (2020) methodology to our model and use daily U.S. death data to derive estimates discussed in sub-section 4.1 in the main text. The SEIR model in discrete time is described by the following set of equations:

$$\begin{aligned}
\Delta S(t+1) &= -\beta(t)\cdot I(t)\cdot S(t) && (1)\\
\Delta E(t+1) &= \beta(t)\cdot I(t)\cdot S(t) - \sigma E(t) && (2)\\
\Delta I(t+1) &= \sigma E(t) - \gamma I(t) && (3)\\
\Delta R(t+1) &= \gamma I(t) - \theta R(t) && (4)\\
\Delta D(t+1) &= \delta\theta R(t) && (5)\\
\Delta C(t+1) &= (1-\delta)\theta R(t) && (6)
\end{aligned}$$

Denoting $\Delta D(t+1) = D(t+1) - D(t) = d(t)$

where d denotes daily death flow series as a fraction of the population, and Δd and $\Delta\Delta d$ its first and second differences, respectively.

From (5):

$$\Delta R(t+1) = R(t+1) - R(t) = \frac{d(t+2)}{\delta\theta} - \frac{d(t+1)}{\delta\theta} = \frac{\Delta d(t+2)}{\delta\theta}$$

From (4):

$$\begin{aligned}
I(t) &= \frac{\Delta R(t+1) + \theta R(t)}{\gamma} = \frac{1}{\gamma}\cdot\left(\frac{\Delta d(t+2)}{\delta\theta} + \theta\frac{d(t+1)}{\delta\theta}\right) = \frac{1}{\delta\gamma}\cdot\left(\frac{\Delta d(t+2)}{\theta} + d(t+1)\right)\\
\Delta I(t+1) &= I(t+1) - I(t) = \frac{1}{\delta\gamma}\cdot\left(\frac{\Delta d(t+3)}{\theta} + d(t+2)\right) - \frac{1}{\delta\gamma}\cdot\left(\frac{\Delta d(t+2)}{\theta} + d(t+1)\right) =\\
&= \frac{1}{\delta\gamma}\cdot\left(\frac{\Delta\Delta d(t+3)}{\theta} + \Delta d(t+2)\right)\\
\Delta I(t+2) &= \frac{1}{\delta\gamma}\cdot\left(\frac{\Delta\Delta d(t+4)}{\theta} + \Delta d(t+3)\right)
\end{aligned}$$

From (3):

$$\Delta E(t+1) = E(t+1) - E(t) = \frac{\Delta I(t+2) - (1-\gamma)\Delta I(t+1)}{\sigma}$$

From (2):

$$\frac{\Delta I(t+2) - (1-\gamma)\Delta I(t+1)}{\sigma} = \beta(t)\cdot I(t)\cdot S(t) - \Delta I(t+1) - \gamma I(t)$$

Divide by $I(t)$:

$$\frac{\Delta I(t+2)/I(t) - (1-\gamma)\Delta I(t+1)/I(t)}{\sigma} = \beta(t) \cdot S(t) - \Delta I(t+1)/I(t) - \gamma$$

Re-arrange:

$$\beta(t) = \frac{1}{S(t)} \cdot \left(\frac{\Delta I(t+2)/I(t)}{\sigma} + \left(1 - \frac{1-\gamma}{\sigma}\right) \Delta I(t+1)/I(t) + \gamma \right)$$

Substitute for $\Delta I(t+2)/I(t),\ \Delta I(t+1)/I(t)$:

$$\beta(t) = \frac{1}{S(t)} \cdot \left(\frac{1}{\sigma} \frac{\frac{\Delta\Delta d(t+4)}{\theta} + \Delta d(t+3)}{\frac{\Delta d(t+2)}{\theta} + d(t+1)} + \left(1 - \frac{1-\gamma}{\sigma}\right) \cdot \frac{\frac{\Delta\Delta d(t+3)}{\theta} + \Delta d(t+2)}{\frac{\Delta d(t+2)}{\theta} + d(t+1)} + \gamma \right) \tag{7}$$

We still need to express $S(t)$ from (1):

$$\begin{aligned} \Delta S(t+1) &= -\beta(t) \cdot I(t) \cdot S(t)/N = -\beta(t) \cdot \frac{1}{\delta\gamma} \cdot \left(\frac{\Delta d(t+2)}{\theta} + d(t+1) \right) \cdot S(t)/N \\ S(t+1) &= S(t) \cdot \left(1 - \beta(t) \cdot \frac{1}{\delta\gamma} \cdot \left(\frac{\Delta d(t+2)}{\theta} + d(t+1) \right)\right) \end{aligned} \tag{8}$$

Given the time series of daily deaths d, equations (7-8) above solve for two unknowns in each period: $\beta(t)$ and $S(t)$. Note, again, that $\mathcal{R}_t = \beta(t)/\gamma$

In the computations of sub-section 4.1 of the main text, we posit $1/\sigma = 3$ (Exposed stage), $1/\gamma = 4$ (Infectious stage), $1/\theta = 12.5$ (Resolved stage), $\delta = 0.008$ (Infection Fatality Rate), and initial $S_0 \simeq 1$.